1-1-2016

State Resolved Sliced Imaging Of Infrared Multiphoton Dissociation

Ravin Lakshitha Fernando
Wayne State University,

STATE RESOLVED SLICED IMAGING OF INFRARED MULTIPHOTON DISSOCIATION

by

RAVIN LAKSHITHA FERNANDO

DISSERTATION

Submitted to the Graduate School

of Wayne State University,

Detroit, Michigan

in partial fulfillment of the requirements

for the degree of

DOCTOR OF PHILOSOPHY

2016

MAJOR: CHEMISTRY (Physical)

Approved By:

Advisor	Date

DEDICATION

~To my mother, father and wife Lakshika~

ACKNOWLEDGEMENTS

I would like to express my deepest appreciation to my supervisor, Prof. Arthur G. Suits, for the precious opportunity given to me to join his group and to pursue my dreams. Thank you very much for the valuable guidance, kindness, support, encouragement and patience throughout this whole period. I am greatly humbled to be able to work with a mentor, who convincingly conveyed a spirit of adventure in regard of the research, and a brain who is enrich with new ideas and technics. I am enormously indebted for everything Prof. Arthur G. Suits for everything he has done to me to be the person who I am now. Without his persistent help and guidance this dissertation would have not been a possible.

Secondly I would like to thank all past and current Suits group members for making this journey a productive and an enjoyable one. I was very fortunate to be able to work with Dr. Argya Dey, who taught me new techniques in the lab and the support given during the experiments. Also I would like to thank former Suits group member Dr. Nuradhika Herath for the supports given in numerous ways in the lab to gain the experience to work with the Beta machine. I am thankful to Dr. Bernadette Broderick for all the helps and her friendship as being my neighbor in the lab.

I am grateful for the support I received from the department of chemistry of Wayne State University and University of Missouri, Columbia during the studies. This journey would have not been an easy one without their enormous administrative support. I want to thank Melissa Barton, Diane Kudla, Bernie Meisik, Kellie Lauder, Erin Bachert, and Jackie Baldyga for all the helps in numerous ways. I like to extend my gratitude to Nestor Ocampo for bearing the pain and being there for me whenever I had any technical issues.

I take this opportunity to thank my committee members Prof. Wen Li, Prof. Vladmir Chernyak, Prof. Zhongwu Guo, and Prof. Xiang-Quiang Chu for spending their valuable time for

me and being there for me to make this journey a successful one. I am also really thankful to be able to teach with Dr. Barbara Munk, who was so much patient and helpful with me while teaching how to be a great teacher.

I would like to thank my college friends Nirosh Attanayaka, Kasun Kosgahakubura, Nuwan Jayawardana, Chamra Sumanapala, Tharidu Somapala and Sasanka Warnakula for being such good friends when I was having a difficult time. I am forever in debt for my friends for carrying me through all the hurdles and supporting me as true genuine friends who are fortunate to have.

Last but not least I would like to thank my family for all the support given for me to make this journey a success. A special thank goes to my mother for being the hero and supporting me in every possible way to be a better man. I hope you will be the proudest mom I have ever seen. I am really fortunate to have my best friend as my wife and I would like to thank her for all the sacrifices, understanding, love and courage which she made towards me to achieve this goal.

TABLE OF CONTENTS

LIST OF TABLES

LIST OF FIGURES

PREFACE

This Thesis is based on the following publications:

1. Arghya Dey, **Ravin Fernando**, Chamara Abeysekera, Zahra Homayoon, Joel M. Bowman, and Arthur G. Suits. "Photodissociation dynamics of nitromethane and methyl nitrite by infrared multiphoton dissociation imaging with quasiclassical trajectory calculations: Signatures of the roaming pathway." *The Journal of chemical physics* 140, no. 5 (2014): 054305.

2. **Ravin Fernando**, Nuwandi M. Ariyasingha, and Arthur G. Suits. "Imaging NO elimination in the infrared multiphoton dissociation of nitroalkanes and alkyl nitrites." *Chemical Physics Letters* 645 (2016): 76-83.

3. **Ravin Fernando**, Arghya Dey, Bernadette M. Broderick, Bina Fu, Zahra Homayoon, Joel M. Bowman, and Arthur G. Suits. "Visible/Infrared Dissociation of NO3: Roaming in the Dark or Roaming on the Ground?." *The Journal of Physical Chemistry A* 119, no. 28 (2014): 7163-7168.

4. **Ravin Fernando**, Chen Qu, Joel M. Bowman, Robert W. Field, and Arthur G. Suits. "Does Infrared Multiphoton Dissociation of Vinyl Chloride Yield Cold Vinylidene?." *The journal of physical chemistry letters* 6, no. 13 (2015): 2457-2462.

CHAPTER 1 INTRODUCTION

1.1 Introduction

Molecular reaction dynamics is a field which uniquely relates the macroscopic properties of molecules with their molecular and atomic level behaviors. In doing so, a thorough picture of key fundamental properties is obtained through detailed experimental and theoretical studies, and ultimately, meaningful information about the macroscopic features of the world in which we live are revealed.

At its birth, chemical reaction dynamics sought to unravel the series of chemical changes that occur in environments as a consequence of complex elementary chemical reactions. Over the course of the last several decades, new techniques have enabled the study of such reactions in incredible detail, allowing for a clearer understanding of such fields including astrochemistry, drug chemistry, combustion chemistry, and protein mechanics. These detailed probes used in the field of molecular reaction dynamics have yielded great insight into molecular level behaviors, and have paved the way to a deep understanding of the driving forces of a system which govern the outcome of a chemical reaction.

In order to understand elementary chemical reactions, studies must be performed under well-defined laboratory conditions to independently isolate the reactants, reactive intermediates, and products of a reaction. With the development of laser technology in the last several decades, novel techniques have been designed to explore the dynamics of molecular dissociation. Dissociation events are often a key component in many chemical reactions and are of keen interest for many fields of chemical science. Evolution in the computational field simultaneously with the development of advanced experimental techniques has complimented molecular reaction dynamic studies with the ability to explore the molecular potential energy surfaces. The

field of molecular reaction dynamics has developed enormously with the support of theoretical calculations. Specially, quasi-classical trajectory calculations (QCT) using global potential energy surfaces (PES) have expanded the details which we determine about the dissociation dynamics of molecules.

In this dissertation we have focused on studying unimolecular dissociation of molecules from the ground electronic state under collisionless conditions. The detection method used for these studies is capable of probing and determining energy, orientation, and alignment of their individual quantum states of the reactant and product species. Specifically, experiments were carried out to understand the predominant pathways, branching ratios, energy barriers, and dissociation mechanisms. The first of these studies were performed on nitromethane and methyl nitrite to clarify the dissociation dynamics via the isomerization channel. Furthermore, NO_3 was studied to understand the excited state involvement for roaming dissociation; finally, investigations were conducted on vinyl chloride to determine if this system could be used as a route to produce rotationally and vibrationally cold vinylidene.

1.2 Infrared Multiphoton Dissociation

Infrared Multiphoton Dissociation (IRMPD) is a technique that was developed in 1970s to study bond selective chemistry in the early stages of dynamical studies. This method was developed with the idea of dissociating a polyatomic molecule through a selective vibrational degree of freedom.[1-3] In the early stages, mass spectroscopy was used to detect the primary dissociation products from the parent molecule.[4, 5] This data could be used to reveal the correlation between the excited vibrational mode and the ensuing dissociation.[6] It was understood that there were several important questions to be answered: What are the differences between the single photon excitation and multi photon excitation? How does a molecule reach

the dissociation continuum through discrete mode and quasicontinuum excitation? Do molecules become excited via a single vibrational mode or randomize into other vibrational modes? Most of these questions can be answered by analyzing the final products by measuring their angular and velocity distributions. As such, MPD experiments were carried exclusively in order to answer these questions.

The discovery of IRMPD engendered hopes of mode-selective dissociation and isotopically selective bond dissociation of polyatomic molecules with intense CO_2 laser pulses due to the difference in the bond dissociation energy.[7, 8] Soon it was realized that IRMPD could not be employed to achieve bond selective chemistry because of the rapid internal vibrational relaxation (IVR). Vibrational relaxation occurs in the pico second time scale and it suppresses the vibrationally selective IR photon absorption in the nano second scale.[9] However, the advent of the technique enabled the study of the nascent photofragments from photodissociation of molecules on the ground electronic state and revealed structural information of the parent molecule.[1] At the outset, IRMPD was used to study the properties of charged species with trapped-ion mass spectrometry.[10, 11] Y. T. Lee and co-workers used this technique with photofragment translational spectroscopy to study different reaction pathways originating from unimolecular dissociation of simple polyatomic molecules such as SF_6[12, 13], acetone[14], acetic acid[15], halogenated hydrocarbons[16-18], nitromethane[19, 20], and esters.[21] These studies revealed several elementary processes such as intramolecular energy transfer, isomerization, molecular elimination, and simple bond fission.

Rapid absorption of infrared photons leads the molecule to dissociate at the dissociation threshold of the ground electronic state. The statistical theories of unimolecular dissociation that assume the free flow of vibrational energy in the dissociating molecule are used to describe the

dissociation process and to elucidate the products.[22] Even though the IRMPA vibrational population cannot be characterized by temperature, there is no significant difference between thermal population and IRMPA population. [23] The products obtained from IRMPD in a collision-free environment resemble those from the thermal decomposition of the particular molecule.[24, 25] Exclusion of the excited electronic state during the dissociation makes this technique a better method to study the roaming reactions.

1.3 Roaming Reactions

Roaming reactions are a newly reported class of unimolecular decomposition of energized molecules into radical products near the dissociation threshold followed by intramolecular abstraction or isomerization to distinct and sometimes unexpected products.[26, 27] Roaming dissociation was initially reported in the photodissociation of formaldehyde. [28-30] Since then, this class of dissociation has been reported with several other molecules such as acetone[31], acetaldehyde[32-34], NO_3[35-38], ethyl nitrite[39], HOONO[40], C_2H_4OH[41], $(CH_3)_2O$[42], CH_3NH_2[43], and NH_3.[44] To understand the roaming mechanism, one must first consider transition state theory (TST). TST is a universally recognized method to describe and predict the reaction rates of chemical reactions. TST uses simplified assumptions of dynamical behaviors to calculate the reaction rates based on statistical mechanics and quantum theory. Thus, a complex reaction is a series of bimolecular reactions or unimolecular dissociations, which proceed via well-defined transition states. These transition states are used in the assumptions and calculations of TST. However, ion imaging experiments of unimolecular dissociation of formaldehyde by the Suits group in combination with quasi classical trajectory calculations from the Bowman group demonstrated that a molecule can undergo a frustrated dissociation near the radical dissociation asymptote energy barrier while avoiding the

conventional transition state geometry but eventually end up as a molecular product. This unusual decomposition of a molecule near the dissociation threshold via the radical channel while avoiding the conventional transition state followed by intramolecular abstraction gives vibrationally excited molecules as a product during dissociation. This type of unusual dissociation of the molecules is called the “roaming dissociation”.

A related process to roaming dissociation is roaming mediated-isomerization. This phenomenon occurs in the isomerization step of the decomposition channel of a molecule. Nitrobenzene is the first molecule where roaming mediated isomerization was identified.[45] Nitromethane was subsequently studied as another system where roaming mediated isomerization predominates during the dissociation.[46-48] These systems show a significant contribution of the NO loss channel during the dissociation. In a study of nitromethane dissociation with IRMPD done by Y. T. Lee and co workers in 1986, they found out that 40% of nitromethane dissociates via the isomerization of nitromethane to methyl nitrite prior to dissociate into NO as a product.

Most of these roaming dissociations and roaming mediated isomerizations originate from the ground electronic state. Roaming in the case of NO_3 is unusual, as it is the first molecule where roaming dissociation was observed in an excited electronic state. Michael Grubb and co-workers experimentally identified the roaming dissociation of the NO_3 molecule.[36] After this experimental evidence, Morokuma and co-workers investigated the dissociation dynamics of the NO_3 molecule. They determined that after exciting NO_3 to the D_3 bright state, it is relaxed through D_3/D_2, D_2/D_1 conical intersections to the optically dark D_1 state. Indirect dissociation through a nonadiabatic transition to the D_0 surface gives the vibrationally hot O_2 products, while direct dissociation on the D_1 surface give vibrationally cold O_2 as a product.

Even though NO_3 shows an unusual behavior during the roaming dissociation with involvement of excited electronic states, it is believed that roaming dissociations predominate from the ground electronic state. IRMPD with a state selective detection method is the effective way to study roaming dissociations since most of these dissociations originate from the ground electronic state. Experimental techniques used in these studies are discussed in detail in the next chapter.

CHAPTER 2 EXPERIMENTAL METHODS

2.1 General Overview

Collision theory is a theory which explains the reaction rates of an elementary reaction qualitatively. This theory is capable of explaining how certain reactions take place, how reaction rates differ for different reactions, how reaction rates vary with different physical properties like pressure, volume, and temperature. In order to understand an elementary reaction completely, it is important to understand both qualitative and quantitative nature of the particular reaction. Therefore, unimolecular dissociations of reactions are studied under collisionless conditions to explore both qualitative and quantitative nature of reactions. Molecular beam experiments are carried out in the vacuum to fulfill the requirement to study the photodissociation of molecules under collisionless conditions.

A reaction consists of a series of elementary reactions, which can be studied in detail by studying the molecular level mechanisms of elementary reactions and physical processes. The studies about unimolecular dissociations require the knowledge about the quantum states of the initial reactants and final products, their velocity, and the angular distribution. These information relates to the reaction enable to study dissociation mechanism and dynamics of the particular reaction. Unimolecular photodissociation like described above, can be described using a reaction as below,

$$ABC_{(e,v,j)} + h\nu \rightarrow AB_{(e,v,j,)} + C_{(e,v,j,)} + KE \qquad R1$$

where *e,v,* and *j* are electronic, vibrational, and rotational quantum states and KE is the kinetic energy of the product. If the reactants are produced in well-defined states, by measuring the quantum states and velocity distribution of the products, dynamics of the elementary reactions can be studied in great detail using the conservation of energy and momentum. Recoil velocity is

the scattered direction of a product after a photochemical event relative to the lab frame. There have been numerous techniques which measure the recoil velocity of a product respect to the lab frame. In this dissertation we have discussed the studies carried out concerning unimolecular photodissociation of complex reaction systems by measuring the velocity distributions of products using velocity map imaging. Velocity map imaging technique combined with the time of flight (TOF) method to isolate the desired product is used as the detection method.[49] Translational energy and the velocity of the co-products can be calculated using the conservation of linear momentum and energy.

As described earlier, these calculations are highly dependent on the state distribution of the reactants. To make this step really simple, reactants are introduced to the source chamber as molecular beams which undergo a supersonic expansion. This is accomplished by seeding the reactants in a noble gas, which is coexpanded from a nozzle source and collimated by a skimmer. During the expansion, the enthalpy of the gas molecules behind the nozzle is transferred to the translational energy of the molecules. Rotationally and vibrationally cold reactants during the expansion have a narrower velocity distribution relative to the laboratory frame, which can aid in the study of the unimolecular photodissociation as well-defined reactants. The process become less complicated by introducing the reactants in known or well-defined states. If we think about the dissociation of ABC molecule into AB and C as products in a unimolecular photodissociation, the velocity distribution of the products in the center-of-mass frame relate to each other as below:

$$\frac{1}{2}m_{AB}v_{AB}^2 + \frac{1}{2}m_C v_C^2 = E_{h\nu} + E_{ex}(i,f) = \frac{1}{2}\mu v_r^2 \qquad \text{(E1)}$$

m_{AB} = mass of AB

v_{AB} = velocity of AB

m_C = mass of C

v_C = velocity of C

E_{hv} = energy of the photon

$E_{ex}(i,f)$ = energy release of the reaction from reactant state *i* to product state *f*

μ = reduced mass of the products

v_r = relative velocity of the products

If v_r is the relative velocity of the product AB and C after the photodissociation, $v_r = v_{AB} - v_C$, then v_{AB} and v_C can be written as follow.

$$v_{AB} = -\left(\frac{m_C}{m_{AB}+m_C}\right) v_r \quad \text{(E2)}$$

$$v_C = \left(\frac{m_{AB}}{m_{AB}+m_C}\right) v_r \quad \text{(E3)}$$

By measuring the velocity of a single product, the velocity distribution of the counter part and the total translational energy distribution of the products can be calculated using the conservation of momentum and energy. In the experiments discussed in this dissertation, a single product from the photodissociations is state selectively ionized with resonance enhanced multi-photon ionization (REMPI) technique. The development of high-resolution lasers with great tunability has increased the utilization of this technique. In REMPI, a molecule is excited to its' resonance states with *nhv* photons where *n* is an integer (gereally1, 2 or 3) and another extra photon to ionize the molecule or atom to be able to detect. These ions are then detected using a micro channel plate (MCP) coupled to phosphor screen. The following section describes the detection system in detail.

2.2 DC Slice imaging

The ion imaging technique was invented by Chandler and Houston in 1986.[50] In ion imaging experiments, supersonically expanded molecules are photodissociated using a photolysis

laser and the concerned products are quantum selectively ionized. This ion cloud travels through a field-free time of flight (TOF) tube on to a MCP coupled with a fast phosphor screen. In order to obtain accurate determination of intensity of the ion distribution, a two dimensional intensified ion array was used. These two-dimensional images were reconstructed to obtain the three-dimensional velocity distribution of the products.

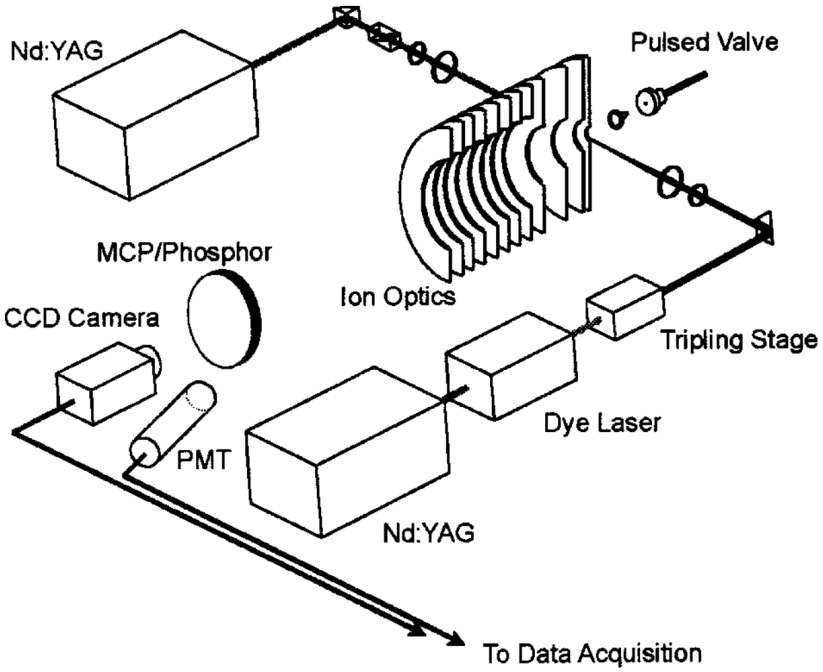

Figure 2.1: Schematic representation of the experimental setup for the dc slice imaging. Adapted from D. Townsend *et. al. Rev. Sci. Instrum.,* 74, 2530 (2003)

In 1997, a significant advancement of molecular imaging was achieved through the development of velocity map imaging. The high resolution, velocity map imaging (VMI) technique was pioneered by Eppink and Parker as a developed version of the traditional ion imaging technique.[49] Velocity map imaging has become the standard method for studying photoinitiated fragmentation, ionization, electron detachment, and active scattering processes. In the velocity map imaging technique, the expanded photofragmented three-dimentional (3D) distribution is imaged on to a two-dimentional (2D) position sensitive detector. Abel

transformation, Onion Peeling, BASEX or any related techniques are used to reconstruct the 2D image to obtain the original 3D distribution. Even though this technique has been successfully applied in a number of experiments, there are two disadvantages with this technique. The requirement of a cylindrical symmetric axis parallel to the imaging plane to use the reconstruction techniques is the first disadvantage. This reason limits the laser polarization which can be used for the experiments. The second disadvantage is the introduction of artificial noise

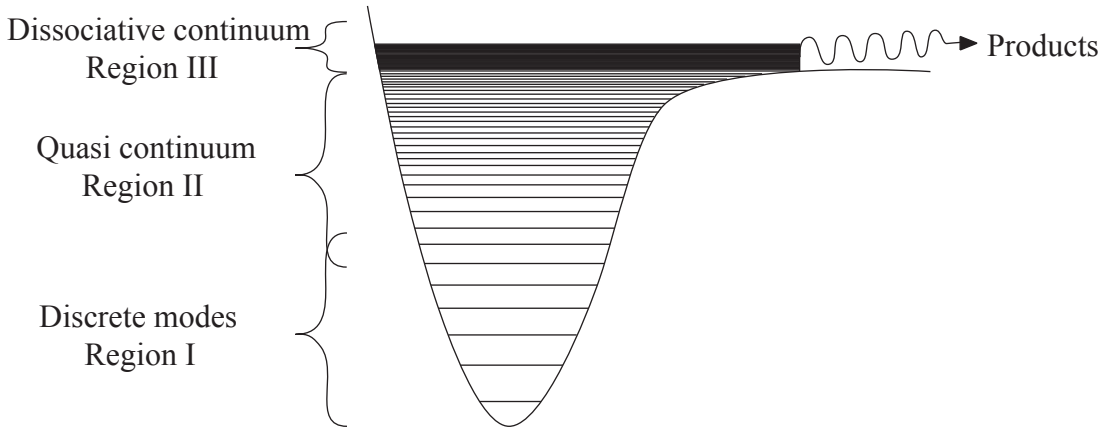

Figure 2.2: Schematic representation of rotational and vibrational levels distribution in key regions during IRMPD.

to the reconstructed image during the reconstruction, which leads to a loss of experimental resolution. With the attempts to overcome these disadvantages, it was understood that the central slice of the ion cloud contains the full angular and velocity distribution. In principle, by detecting only the central slice, the need of the Abel transformation method to reconstruct the image can be eliminated. Kitsopolous and co-workers used a pulsed electric field to expand the ion cloud followed by field free expansion to detect the central slice of the ion cloud.[51-53] Even though this technique was capable of detecting only the central slice, it decreased the resolution of the image because of the fine mesh grid used to apply the electric field. The direct current (DC) slice imaging technique which was developed in the Suits group uses no mesh grid to apply a pulsed

electric field.[54] As a result, this technique preserves the pure velocity map conditions and increases the resolution of the image.

The machine used to study the photodissociation (Figure 2.1) discussed in this dissertation consists two chambers, the source chamber and the main chamber, which are maintained at $1x10^{-5}$ torr and $1x10^{-7}$ torr respectively. The seeded molecular beam is introduced to the source chamber using a solenoid pulse valve (General Valve Series 9) of nozzle diameter 0.8 mm with a pulse duration of 300 μs. It was operated at a 10 Hz repetition rate. The supersonically expanded beam is collimated and introduced to the main chamber through a 1 mm skimmer. Then the molecules are photodissociated between the repeller and the extractor followed by ionization using the REMPI scheme. Then the product ions are accelerated through a field free 80cm long TOF tube onto a 120 mm dual channel micro channel plate coupled to a P-47 phosphor screen. A CCD camera (USB 2 uEye SE,IDS) is used to view the resulting images and the snaps of the velocity distributions of the photochemical events are acquired using a NuACQ program.

2.3 Heated molecular beam

In the early stages, molecular beam experiments were identified as the most appropriate way to study the MPD of polyatomic molecules under collisionless conditions.[55] To dissociate a molecule on the ground electronic state vibrational threshold, it should be excited to the dissociative continuum through discrete mode and quasicontinuum region. A molecule should absorb roughly 20-30 IR photons in order to reach the dissociation continuum and to be able to dissociate into products. Because of the anharmonicity, energy gap between rotational and vibrational level decreases as the quantum number increases. Hence, exciting a molecule to the dissociative continuum starting from the $\upsilon=0$ level using a single wavelength becomes

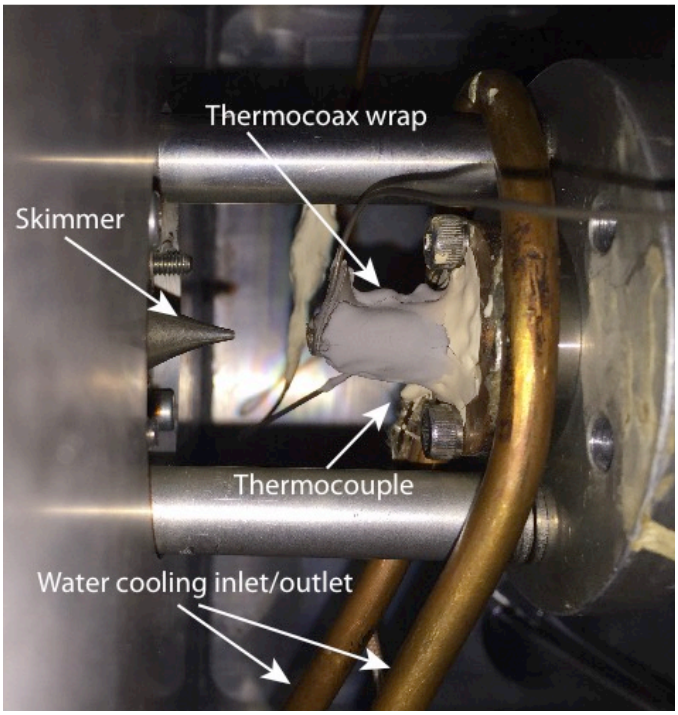

Figure 2.3: Source chamber of Beta.

incompetent. Since there is no significance difference between the infrared multiphoton absorbed (IRMPA) population and thermal population, in IRMPD, molecules are excited in the discrete mode (region I) (Figure 2.2) by heating the molecular beam. A CO_2 laser beam excites the molecules in the quasi-continuum region and the molecules dissociate once they are excited into the dissociative continuum.

To heat-up the molecular beam, a Cu tube with a 0.5 mm bore diameter was fitted to the basal of the general pulsed valve. The Cu tube was wrapped with thermocoax (SEI 15/50), which is heated up by supplying a DC voltage. (figure 2.3) The temperature of the beam is controlled by adjusting the supplied voltage and a thermocouple is attached to the tip of the Cu tube to measure the temperature of the nozzle. The temperature of the nozzle was observed with the signal strength and the temperature of the heating coil was kept lowered as much as possible to get rid of the background signal. The basal Cu plate is wrapped with a Cu tube to water-cool the pulsed valve. Since the distance between the orifice and the skimmer changes with the addition

of the heated nozzle, the distance between the skimmer and the tip of the heated nozzle was optimized in order to gain the maximum resolution of the ion distribution.

2.4 Laser System

IR wavelengths for the experiments were produced using a TEA-CO_2 laser (GAM laser, EX100/60). This laser system is able to generate 56 separate laser lines in the wavelength region from 9.2 -11.2 μm. The output wavelengths were confirmed using a CO_2 spectrum analyzer (Macken Instruments). For each experiment, the wavelength that was selected depended on the particular resonance in the target system that gave the strongest signal with minimum laser power.

UV/Visible wavelengths were produced by sum frequency mixing and second harmonic generation of output laser beams from commercially available dye laser system (Sirah, Precision Scan). These dye lasers were pumped using the second and third harmonic output of Nd-YAG lasers (Quanta-Ray, Pro 250), 532 and 355 nm respectively. Wavelengths were measured using the wave meter (WaveMaster). Power of the lasers were optimized to maximize the signal strength and to minimize the background in the experiment.

2.5 Instrument Calibration

Velocity distributions for the products were calculated using the calibration factor, which is obtained by collecting an image for a known transition. The radial distance from the center of the image is proportional to the velocity of the product. The velocity (m/s) for a pixel was calculated using the calibration image and that value was used to calculate the unknown velocity distributions of the products. For the experiments discussed in this dissertation, setup was calibrated using the photodissociation of NO_2 into NO (Q_1, J'=12) and O (^1D). Wavelength used

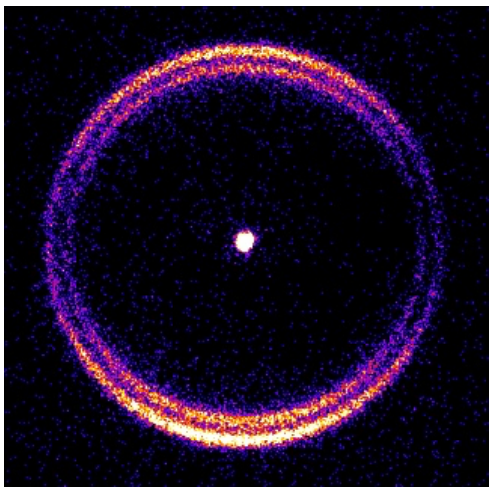

Figure 2.4: Image for the NO (Q1, J'=12)

for this calibration step is 226.102 nm (44227.74 cm^{-1}). Calculation of the calibration is shown below,

$NO_2 + h\upsilon \rightarrow NO\ (J'=12) + O\ (^1D)$ (R2)

Dissociation energy (D_0) of this channel is 40996.4 cm^{-1}. The collected images for calibration consisted two components since Q_1, J'=12(fast component) transition is overlapped with the Q_{21}, J'=20 (slow component) transition. Calculations were done for both transitions and an average value was used as the calibration factor. Rotational energy of NO at J'=12 is (fast component),

$E_{rot} = BJ(J+1) - DJ(J+1)2$

$E_{rot} = 1.6706 \times 12\ (13) - 0.54 \times 10^{-6} \times 12^2 \times 13^2$

$E_{rot} = 260.6\ cm^{-1}$

Remaining energy available is distributed among NO and O as translational energy,

$E_{remaining} = 44227.74 - 40996.4 - 260.6\ cm^{-1}$

$E_{remaining} = 2970.74\ cm^{-1} = 35.531\ kJ/mol$

Reduced mass of the system, μ (NO + O) = $\frac{m_{NO}\, m_O}{m_{NO}+m_O} = 10.435$ g/mol

$E_{remaining} = \frac{1}{2}\mu v_{rel}^2$

$35.530 \times 10^{-3} = \frac{1}{2} \times 10.435 \times 10^{-3} \times v_{rel}^2$

$v_{rel} = 2609.556\ ms^{-1}$

$v_{NO} = v_{rel} \frac{m_O}{m_{NO}+m_O} = 2609.556 \times \frac{16}{46}\ ms^{-1}$

$v_{NO} = 907.67\ ms^{-1}$

Measured number of pixels for the fast component from the figure 2.4 is 201 pixels. Hence, calibration factor calculated from the fast component is 4.51 ms^{-1}/pixel. For the slow component, rotational energy of NO at Q21, J'=20 transition is,

$E_{rot} = BJ(J+1) - DJ(J+1)2$

$E_{rot} = 1.7111 \times 20\ (21) - 10.23 \times 10^{-6} \times 20^2 \times 21^2$

$E_{rot} = 840.19\ cm^{-1}$

Remaining energy available is distributed among NO and O as translational energy,

$E_{remaining} = 44227.74 - 40996.4 - 840.19\ cm^{-1}$

$E_{remaining} = 2391.15\ cm^{-1} = 28.598\ kJ/mol$

$E_{remaining} = \frac{1}{2} \mu v_{rel}^2$

$28.598 \times 10^{-3} = \frac{1}{2} \times 10.435 \times 10^{-3} \times v_{rel}^2$

$v_{rel} = 2341.196\ ms^{-1}$

$v_{NO} = v_{rel} \frac{m_{NO}}{m_{NO}+m_O} = 2341.196 \times \frac{16}{46}\ ms^{-1}$

$v_{NO} = 814.33\ ms^{-1}$

Number of pixels measured from the figure 2.4 for the slower component is 183 pixels and average calibration factor calculated using the slower component is 4.45 ms^{-1}/pixel. Hence, the

average calibration factor calculated from the figure 2.4 is 4.48 ms^{-1}/pixel. Radial distribution of the image is dependent on the voltages used to focus the ion optics. Therefore, calibration factor was calculated whenever voltages were changed to increase the resolution of the image. Experiments studied using these experimental techniques and conditions are discussed in the following chapters.

CHAPTER 3 PHOTODISSOCIATION DYNAMICS OF NITROMETHANE AND METHYL NITRITE BY INFRARED MULTIPHOTON DISSOCIATION IMAGING WITH QUASICLASSICAL TRAJECTORY CALCULATIONS: SIGNATURES OF THE ROAMING PATHWAY.

3.1 Introduction

Roaming reactions are a newly reported class of unimolecular reactions that involve near-dissociation to radical products followed by abstraction or isomerization leading to distinct and sometimes unexpected products.[26, 27] Roaming was initially reported in formaldehyde photodissociation and has since been seen in many systems.[28] Roaming-mediated isomerization has been invoked in dissociation of nitrobenzene[45] and nitromethane[46-48] to account for the significant yield of the NO loss channel in these systems. To date, however, in primary photodissociation studies of roaming dynamics, only UV excitation has been used to prepare excited molecules for subsequent investigation. Since reactions involving roaming mechanisms largely arise from the ground electronic state, IRMPD studies can be very helpful in providing unambiguous information about such processes.

Nitromethane (CH_3NO_2) is the simplest homologue in the family of nitroalkanes that have been important as energetic materials in the form of propellants and explosives. The photodissociation dynamics of nitromethane have drawn significant attention and have been studied extensively using ultraviolet excitation from the ground electronic state.[56-58] A key early photofragment translational spectroscopy study by Wodtke, Lee and co-workers using IRMPD[20] reported 40% branching to NO loss. This large percentage implied efficient isomerization to the nitrite prior to dissociation:

$$CH_3NO_2 + nhv \rightarrow CH_3ONO* \rightarrow CH_3O + NO \qquad (R3)$$

Earlier reports showed that the primary photodissociation channel upon UV excitation produced CH_3 radicals and NO_2, after which the NO_2 may absorb another photon leading to formation of NO and O radical:

$$CH_3NO_2 + hv \rightarrow CH_3 + NO_2 \qquad (R4)$$

Based upon RRKM modeling and the assumed IRMPD kinetics, Wodtke et al. concluded the energy barrier for isomerization was about 5 kcal/mol lower than the C−N bond fission threshold.[20] This would certainly justify the observation of a significant yield of the products from the isomerization channel. This report triggered a series of theoretical calculations on the dissociation dynamics of nitromethane performed by several groups.[59-61] However, none of them could establish the dissociation mechanism via isomerization as an energetically favorable pathway. However, McKee[62] and Saxon[63] et al. did identify a loose transition state leading to the isomerization channel, but at significantly higher energies compared to the radical dissociation pathway. Finally, in 2009, Zhu and Lin[48] revisited the calculations on nitromethane decomposition and located the presence of a loose transition state just below the C−N dissociation limit. The structure of the loose transition state in the isomerization pathway was found to have a striking resemblance to the roaming pathway in the photodissociation of H_2CO.[29] Recently, Homayoon and Bowman[47] performed quasiclassical trajectory (QCT) calculations using a global potential energy surface (PES) for nitromethane decomposition that theoretically documented the roaming-mediated isomerization of $CH_3NO_2 \leftrightarrow$ cis-CH_3ONO. Similar behavior had been inferred in the UV photodissociation of nitrobenzene based on ion imaging and statistical modeling of the product branching and translational energy release on the ground and first triplet excited states.[45] Several features of this isomerization pathway justify the use of the phrase “roaming-mediated”:[47] (1) it involves nuclear reorientation dynamics that

take place at longrange (3–5 Å) and that have an energetic threshold within 1–2 kcal/mol of a bond fission asymptote and (2) trajectory calculations show that this TS is indeed very loose and many trajectories do not go very near this precise configuration.

Imaging provides the complete velocity and angular distribution of the products formed, generally with quantum state selectivity and excellent sensitivity. Since the last decade, velocity map imaging studies have been used extensively in studying the photochemistry of unimolecular dissociation and scattering.[64, 65] The present article demonstrates the first imaging studies combining IRMPD with state-selected imaging. Our focus is on the ground state photodissociation dynamics of nitromethane and methyl nitrite (CH_3ONO). The results provide further support to the recent theoretical studies that propose roaming-mediated isomerization in nitromethane and are in good agreement with the earlier results of Wodtke, Hintsa, and Lee.

3.2 Experimental Section

The carrier gas helium is bubbled through a sample of nitromethane producing a seeded mixture of 3% nitromethane in He. Likewise, in case of methyl nitrite, helium was passed through a bubbler maintained at 196 K forming a ratio of 2% methyl nitrite in He. Methyl nitrite was synthesized by adding 15 ml of methanol to a solution of 12 g of $NaNO_3$ dissolved in 50 ml of deionized water and stirred at room temperature for 5 min. To the resulting solution concentrated HCl was added dropwise through a separating funnel. Methyl nitrite vapors were formed as white fumes, which were condensed to a dark yellow liquid in a bubbler, kept in dry ice/acetone cooling bath (196 K).

The molecular beam was generated by supersonic expansion into the source chamber through pulsed nozzle (General Valves series 9) of diameter 0.3 mm. The pulsed nozzle is fitted to a copper tube having a bore diameter of 0.5 mm that is heated to 573 K which facilitates the

population of a few vibrational levels of the ground state to promote IR absorption. The expanded beam was introduced into the interaction chamber through a skimmer of 1 mm diameter and entered the DC sliced imaging ion optics assembly comprising four electrodes where it intersected two counter-propagating laser beams. The pressure inside the source chamber and the interaction chamber was maintained at 1 × 10−5 Torr and 1 × 10−7 Torr, respectively. On entering the detection chamber the molecular beam interacts with the CO_2 laser beam and the UV beam at ~226 nm. Absorption of many photons from the IR beam from a line-tunable TEA-CO_2 laser leads to dissociation of the molecule on the ground electronic state. The CO_2 laser lines selected for nitromethane and methyl nitrite were 9.6 μm [R(20) line] and 10.2 μm [R(32) line], respectively. Following dissociation, the fragment is state-selectively ionized with the 226 nm beam which was generated from the fundamental output of a pulsed dye laser (Sirah, DCM dye in ethanol) pumped by the second harmonic of a seeded Nd: Yttrium aluminum garnet (Nd:YAG) laser (Quanta Ray, Spectra Physics) which is then mixed with the third harmonic of the Nd:YAG laser. The intensity of the 226 nm beam was reduced to 200 μJ/pulse to eliminate the contribution from photodissociation at 226 nm. The typical energy produced by the CO_2 laser was 100 mJ/pulse and the laser was operated at a frequency of 10 Hz. Both the beams were aligned in the counterpropagating manner and the IR beam was focused onto the molecular beam with a 450 mm focal length ZnSe lens but the UV beam at 226 nm was left unfocused with a diameter of ~5 mm. The temporal overlap between the two laser beams was controlled through a digital delay generator. The CO_2 laser beam was introduced into the chamber 1.2 μs prior to the UV beam. The ions originating from the interaction of the laser beams with the molecular beam were directed through the time-of-flight tube and detected by a 120 mm microchannel plate detector coupled with a fast phosphor screen. The ion image was captured using a USB CCD

camera (USB 2 uEye SE, IDS) and the acquisition was done using our own NuACQ program. The acquired image was analyzed using in-house software to obtain the translational energy distribution for the various rotational levels. The IRMPD REMPI scan was recorded by scanning the UV laser and monitoring the ion signal on the phosphor screen with a photomultiplier tube (PMT). The signal from the PMT was transferred to the PC through an oscilloscope. The REMPI spectrum was generated by acquiring the signal with a custom LabView program.

3.3 Quasiclassical Trajectory Calculations

The PES is a permutationally invariant representation of 114000 DFT/B3LYP energies and precisely reproduces the reaction paths. Fig 3.1 shows the relevant pathways for NO production from nitromethane and methyl nitrite. TS1 is the loose "roaming" saddle point (SP) that connects CH_3NO_2 to cis-CH_3ONO. We note that the importance of a roaming-like transition state in nitromethane was first invoked by Lin[48] to resolve a long-standing discrepancy between experiment and theory on nitromethane decomposition, and subsequently characterized rigorously in Ref. 58. It was shown in that work that isomerization trajectories involved average C–N bond distances of more than 4 Å and vibrational frequencies essentially matching those of CH_3 and NO_2, clearly justifying its characterization as a roaming TS. Although a higher energy tight TS to trans-CH_3ONO (and then without potential barrier to CH3O + NO) was found, it is expected to play a negligible role because it is both energetically and entropically disfavored. It is shown as TS3 in Fig. 3.1. Cis- and trans-CH_3ONO isomerization takes place via TS2. Finally CH_3O + NO products are from O–N bond dissociation of CH_3ONO.

Twenty thousand trajectories were run initiated at cisCH_3ONO at 5 kcal mol−1 relative to the harmonic ZPE of CH_3O + NO. Initial conditions were generated using microcanonical sampling of the initial kinetic energy and with the constraint of zero total angular momentum.

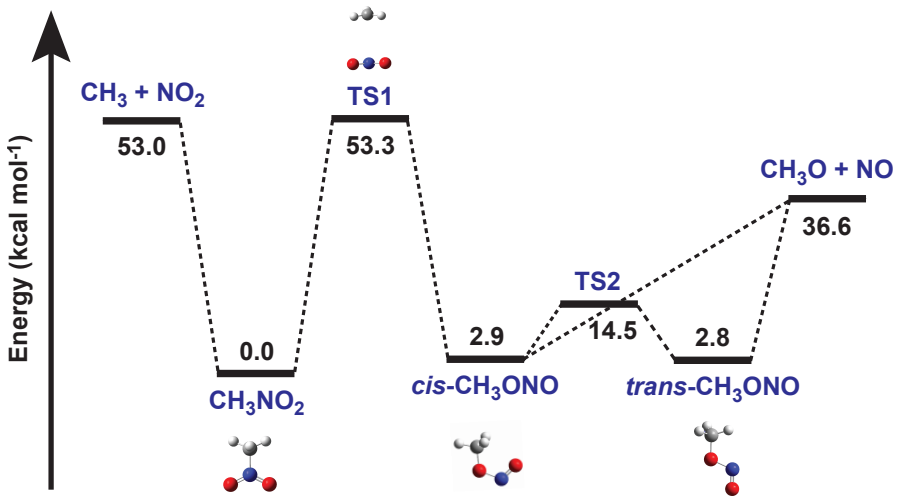

Figure 3.1: Stationary points for different isomerization/dissociation pathways of CH_3NO_2 leading to CH_3O + NO. The energies for the different states are shown relative to the CH_3NO_2 minimum.

Trajectories were run with a maximum of 1 000 000 steps with 0.097 fs step-size. The trajectories were terminated when one of the internuclear distances became larger than 20 bohrs. In the QCT calculations, ZPE issues for the products need to be addressed. Here we adopt the "hard-constraint" in which trajectories are discarded if either fragments NO or CH_3O is formed with less than the ZPE. In addition, we report the vibrational energy distribution of the CH_3O product for trajectories initiated at nitromethane and cis-methyl nitrite with the same total energies for two different energies. Two batches of 20 000 trajectories were run at 60.1 and 86.1 kcal mol−1 energy above the harmonic ZPE of cis-CH_3ONO. In the "Results and discussion" section, the vibrational energy distribution of CH_3O from these trajectories is compared with the results of CH_3O fragments from CH_3NO_2 at the same energies.

3.4 Results and Discussion

The schematic of the PES for the isomerization and dissociation pathways of nitromethane and methyl nitrite obtained by Homayoon and Bowman[47] are shown in Figure

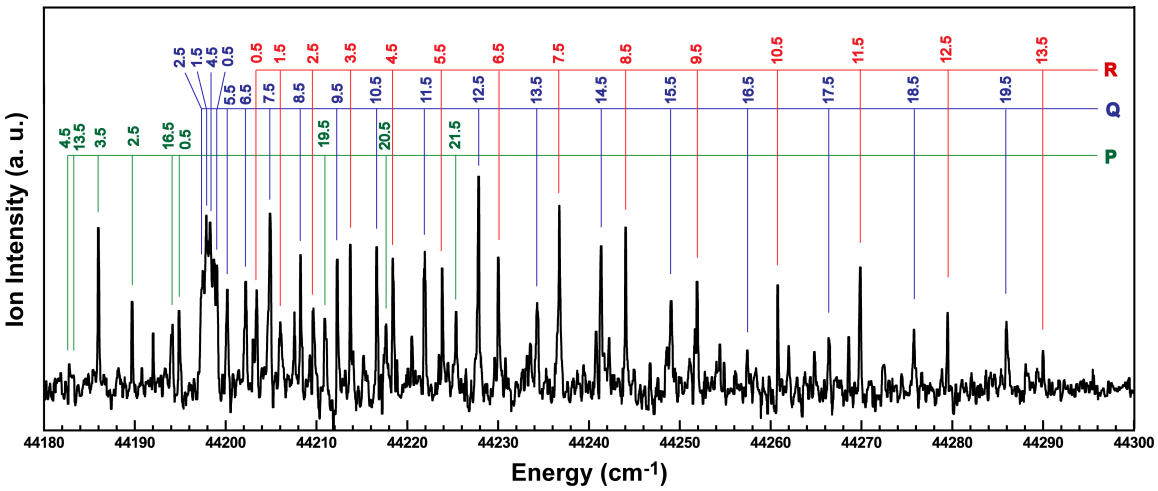

Figure 3.2: Rotationally resolved resonant multiphoton ionization spectrum of nascent NO formed from the IRMPD of nitromethane. The peaks are fitted to the rotational lines for the $A(^2\Sigma^+) \leftarrow X(^2\Pi_r)$ transitions acquired from the LIFBASE program.

3.1. The energies of the various states are shown relative to the global minimum of nitromethane and the energies are not corrected for zero point energy. The schematic shows that the loose transition state leading to isomerization to cis-methyl nitrite is almost isoenergetic with the radical dissociation limit, as is typical for a "roaming" type transition state. This is indicative that a fair amount of branching to the isomerization channel is possible if nitromethane is excited near the dissociation threshold. A REMPI spectrum was recorded for nitromethane on the 0–0 band for the $A(^2\sum^+) \leftarrow X(^2\prod_r)$ transition for the NO and is shown in Figure 3.2. The spectrum displayed in the region 44180–44300 cm^{-1} shows numerous peaks that reflect the rotational distribution of the NO fragment upon dissociation. The peaks are assigned to each rotational transition by comparing the exact position to the simulated spectrum of NO obtained from the LIFBASE program.32 Intense peaks in the lower energy region of the band (44195–44245 cm^{-1}) suggest larger population in the lower rotational levels as expected from IRMPD. The intensities of the isolated spectral lines for the Q and R branch were integrated and divided by the state degeneracy factor (2J + 1), which produced the population of individual states. The logarithm of the population densities for the different rotational levels P(J)/(2J + 1) was plotted against

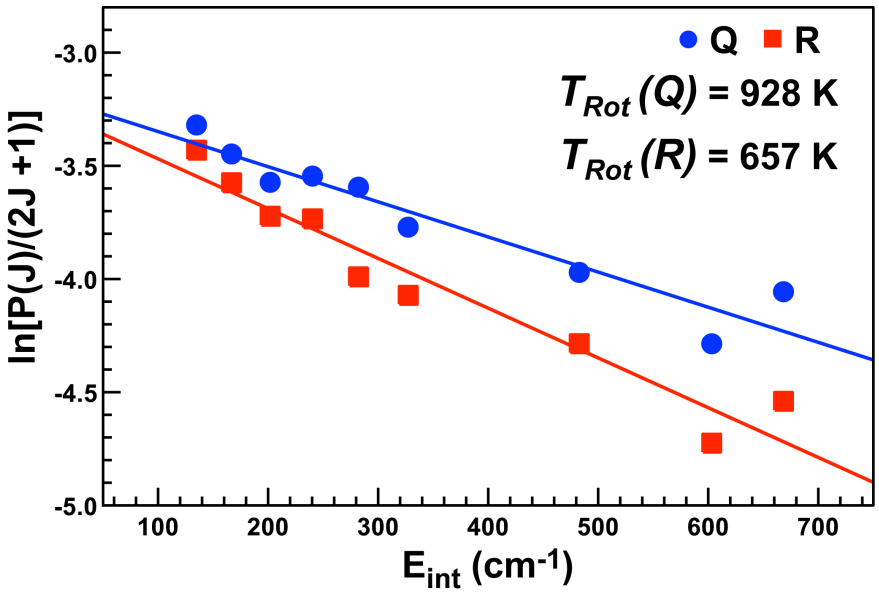

Figure 3.3: Product state distributions for the Q and R branches at different rotational levels of NO obtained from the IRMPD of nitromethane. These are fitted to a Boltzmann distribution to obtain the rotational temperature (T_{Rot}).

internal energy (E_{int}) and the result is shown in Figure 3. A Boltzmann rotational distribution would be described by the equation $P(J) \sim \exp[-E_{int}(J)/kT_{Rot}]$, so the slope in Fig. 3 gives the rotational temperature (T_{Rot}) of the photofragments. The three lowest rotational levels show an elevated population possibly reflecting NO contamination in the beam, and these are excluded from the Boltzmann fit. The rotational temperature (T_{Rot}) of the products obtained from the Q and R branches are 513 K and 411 K, but we emphasize that there is no reason the rotational distributions must exhibit a well-defined temperature. Dissimilar rotational temperatures for the Q and R branch imply that higher rotational levels are differentially populated which denotes preferential occupancy of specific Λ-doublet states. This is confirmed by comparing the intensities of the lines as well as the images, as discussed below. The velocity distribution of the products resulting from IRMPD of nitromethane was obtained from the DC sliced images of the photofragments. DC sliced images of NO fragments were recorded from IRMPD of nitromethane for the Q and R branches for different rotational levels are shown in Figure 3.4.

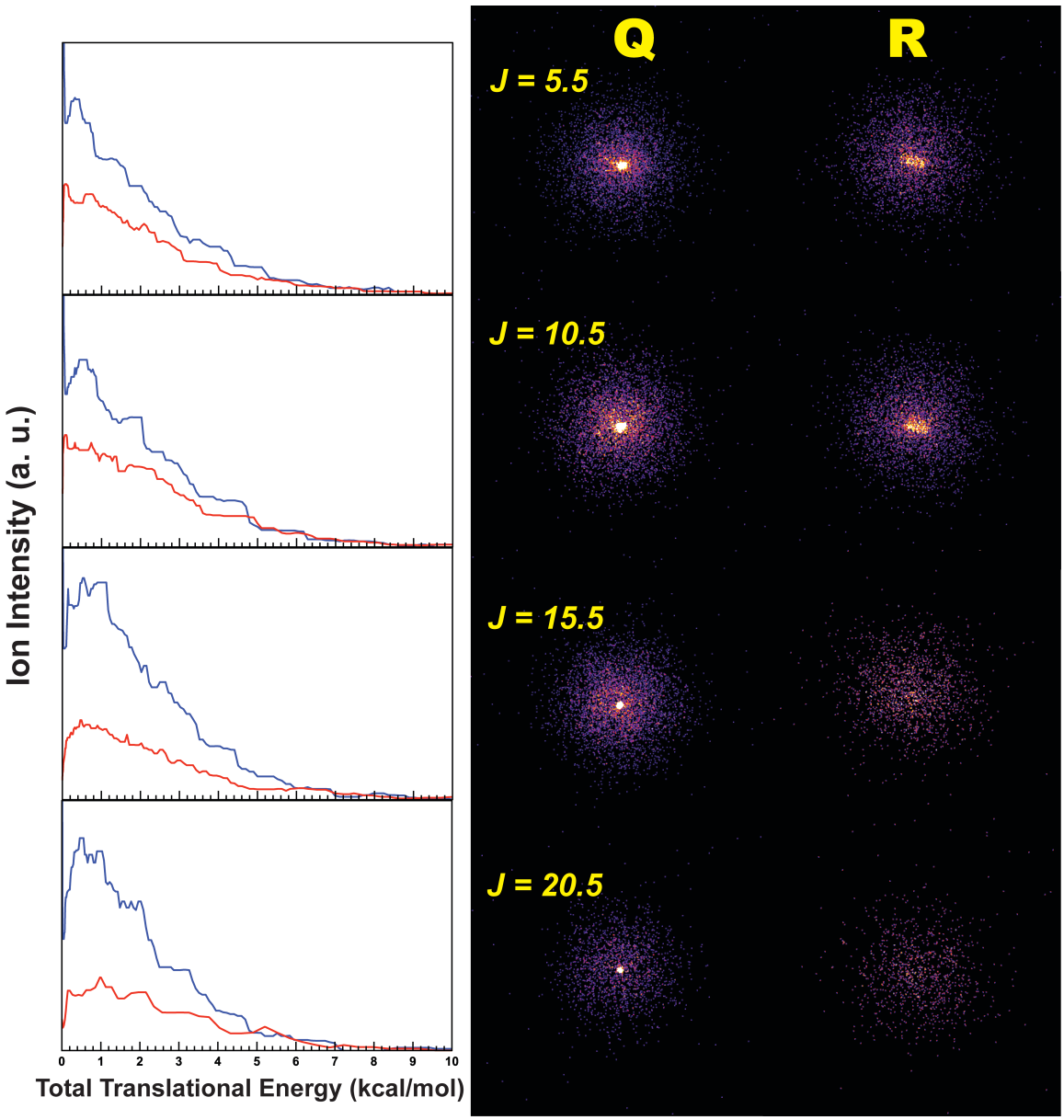

Figure 3.4: Direct current sliced images of NO obtained from IRMPD of nitromethnane. Nitromethane was dissociated by setting the CO2 laser at 9.6 μm and NO was probed around 226 nm. The images were recorded for Q and R branches of different rotational levels which highlights the notable difference in their intensities. (Left) The center-of-mass total translational energies of the fragments for different states of Q (blue) and R (red) branches are also presented.

The images recorded for the nascent NO fragments for different J values probed around 226 nm show only a single component. The brighter regions of the image correspond to higher intensity of the products and the distance from the center of the image gives a measure of recoil velocity

	Nitromethane (CH_3NO_2)		Methyl nitrite (CH_3ONO)	
J value	Q	R	Q	R
5.5	3.3	2.2	1.6	1.4
10.5	3.1	2.4	1.8	1.5
15.5	5.4	2.5	1.1	1.2
20.5	4.7	2.6	0.8	1.2

Table 3.1: Average total translational energy values (in kcal/mol) calculated by probing product NO for the Q and R branches at different rotational levels of nitromethane and methyl nitrite.

of the products. The total translational energies were calculated using conservation of energy and momentum (assuming CH_3O as co-fragment) and the images are displayed alongside. A greater intensity is observed in the images for NO probed via the Q-branch than the R-branch. This disparity indicates that the dissociation favors formation of NO with the π orbital perpendicular to the plane of rotation as discussed further below. The total translational energy distributions for nitromethane show that the energies peak near zero, suggesting barrierless dissociation. Theoretical calculations reveal that methyl nitrite undergoes barrierless decomposition upon isomerization from nitromethane.[47, 48] The average experimentally determined translational energy release ranges from 3.3 kcal/mol to 5.4 kcal/mol for the Qbranch and ranges from 2.2 to 2.6 kcal/mol for the R-branch (see Table 3.1). The limiting value for the total translational energy was found to be $\sim$8 kcal/mol, which is in agreement with the results of the similar IRMPD studies of Lee and co-workers.20 The present IRMPD results are also consistent with the QCT calculations on nitromethane that show the limiting value for the total translation energy of the products to be $\sim$10 kcal/mol at the dissociation threshold (Fig. 4 in Ref. 45). Calculations done by Zhu and Lin[48] suggested that the roaming mediated isomerization

channel dominates at the dissociation threshold, which was later confirmed by the QCT calculations by Homayoon and Bowman.[47] Their branching ratio indicates that NO is the exclusive product via the isomerization channel at the dissociation threshold, with increasing contributions from the radical dissociation channel at higher energies.[47] Observation of a single component in the images also implies that NO is produced from a single channel. Examination of trajectories reveals a roaming/isomcrization pathway[47] that passes near the saddle-point transition state (TS1). On this pathway, the NO_2 fragment moves far from CH_3 (to C–N distances as large 4.6 Å15) and reorients itself and visits the region of isomerization to cis-CH_3ONO followed by O-atom transfer. Evidence of roaming dynamics in formation of NO from photodissociation of NO_3 from both ground and excited state has also been recently reported.[35]

One interesting question to contemplate is whether the interaction of the IR beam with the hot molecule could in- fluence the outcome, i.e., whether some subset of the sampled phase space could preferentially absorb additional IR photons, promoting dissociation via specific paths. In general such issues may be neglected because an energized molecule will spend that bulk of its time with relatively low excitation in any particular mode. During roaming events, however, the molecule may spend a relatively long time in a particular "excursion," perhaps on the order of 10^{-12} s at most. Although this is still very short compared to the lifetime of the system, if the molecule were to absorb very strongly from these geometries, some distortion of the outcome is conceivable. In the present case, however, the roaming geometries will fall out of resonance with the CO_2 laser, (CH_3 and NO_2 have no absorptions in this region) so no effect is expected. This attenuation of absorption during a roaming event could not significantly influence the outcome because the molecule spends only a small fraction of its time in the roaming geometry (or in any TS configuration). IRMPD of methyl nitrite was carried out for comparison

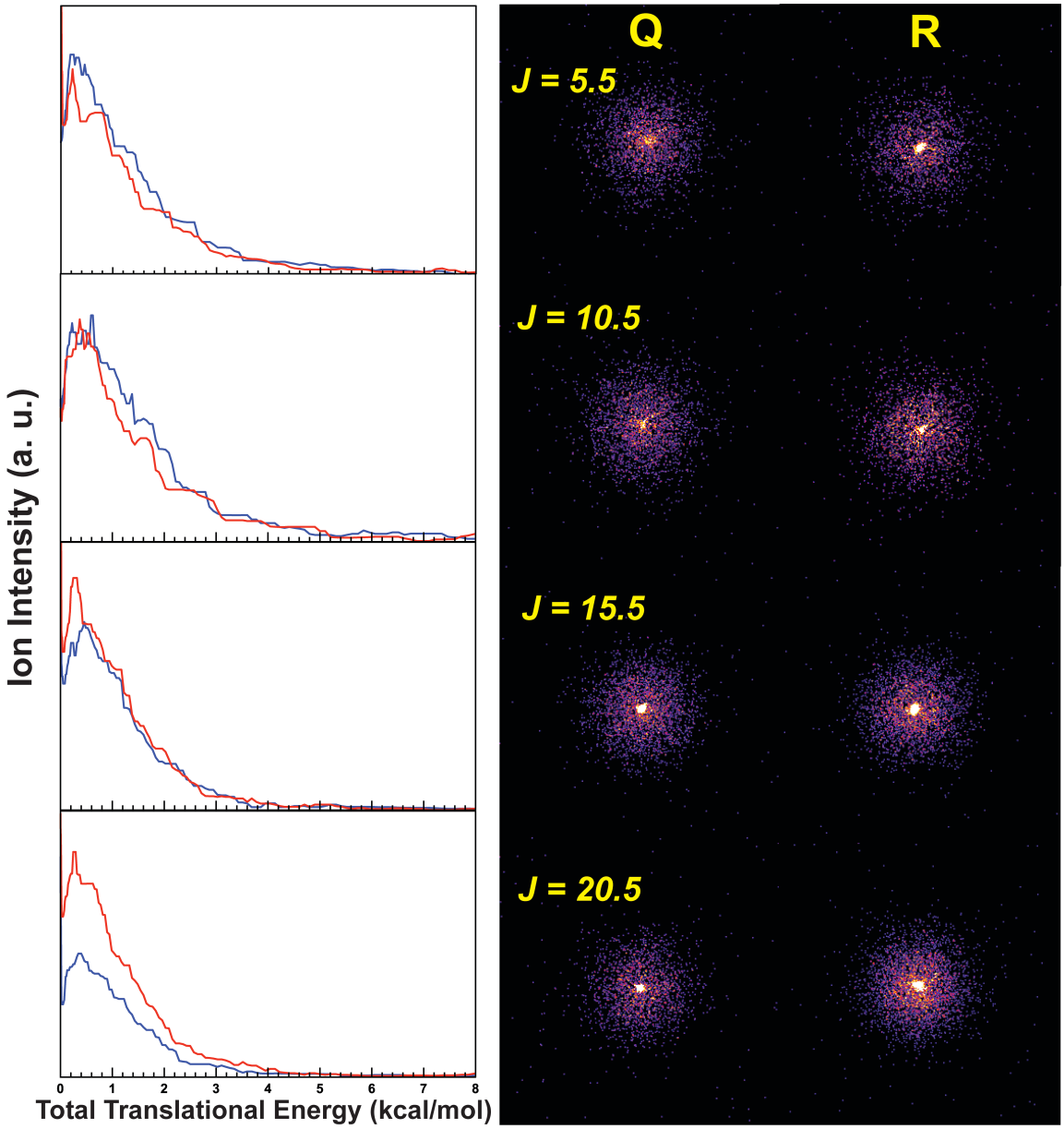

Figure 3.5: Direct current sliced images of NO obtained from IRMPD of methyl nitrite. Methyl nitrite was dissociated by setting the CO2 laser at 10.2 μm and NO was probed around 226 nm. The images were recorded for Q and R branches of different rotational levels. (Left) The center-of-mass total translational energies of the fragments for different states of Q (blue) and R (red) branches are also presented.

with the results obtained from nitromethane. The DC sliced images of IRMPD of methyl nitrite were recorded for the various rotational levels and are shown in Figure 3.5. The images of NO

observed from methyl nitrite look similar to those of nitromethane. The total center-of-mass translational energy for the photofragments was calculated using the conservation of momentum and are displayed alongside images in Figure 3.5. The curves show the total translational energy extending up to 5 kcal/mol and peaking at around 0 kcal/mol. The low translation energy release

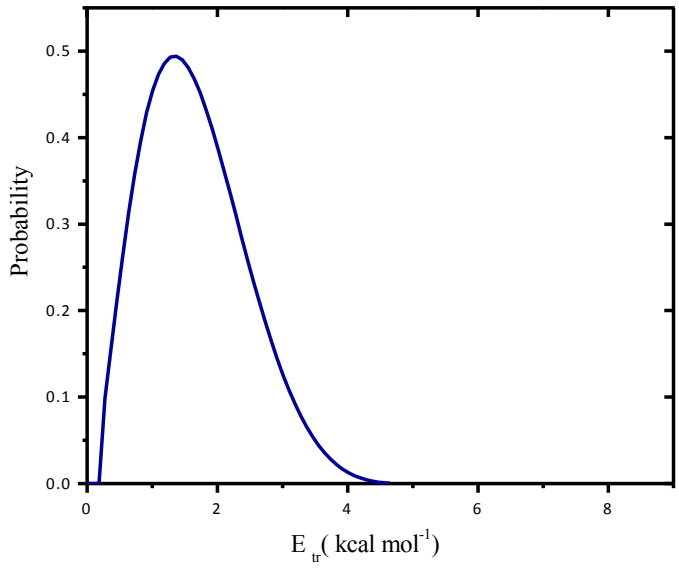

Figure 3.6: Total translational energy distribution of the products formed from dissociation of CH3ONO to CH3O and NO from the QCT calculations. The translational energy was calculated at 5 kcal/mol above the dissociation limit.

of the products is expected as the dissociation of methyl nitrite occurs through a simple fission of O−N bond. The potential energy diagram in Figure 3.1 depicts that both the cis and trans isomers of methyl nitrite undergo barrierless decomposition into CH_3O and NO. The experimental values for the total translational energy show a close resemblance when compared with the calculated total translational energy curve for the CH_3O and NO fragments obtained in trajectory calculations displayed in Figure 3.6. The trajectory data shows a peak at ~1.5 kcal/mol, a limiting value of 4.5 kcal/mol, and an average translational energy release of 1.7 kcal/mol. The total translational energies are calculated at 5 kcal/mol above the NO asymptote. Dissociation of

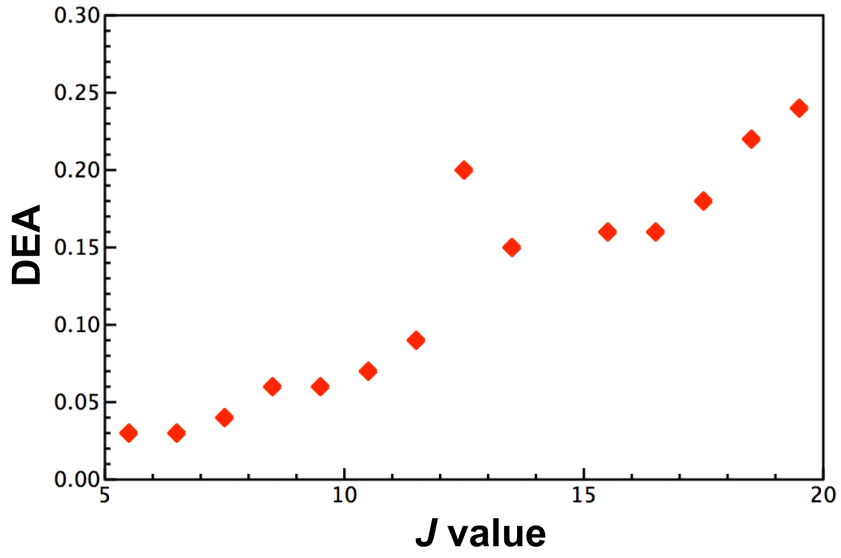

Figure 3.7: Plot of degree of electron alignment against total angular momentum (J) for IRMPD of nitromethane.

methyl nitrite from the ground state proceeds through a simple bond rupture leading to very low translational energy release. The average translational energy observed for the fragments originating from the IRMPD of nitromethane is higher when compared with methyl nitrite. As seen from the PES in Figure 3.1, nitromethane has to overcome the energy barrier for isomerization which provides substantial internal energy to the isomerized methyl nitrite. The isomerized methyl nitrite later dissociates and the energy is in part released in the form of translational energy of the products. Recently, Lin and coworkers studied the thermal decomposition of methyl nitrite and found another competitive pathway resulting in formation of CH_2O and HNO.[66] Their calculations located another roaming transition state 0.7 kcal/mol below the CH_3O + NO asymptote. Future plans are made to study the CH_2O and HNO fragments which can be detected with the newly built Chirped-Pulse FT-microwave spectrometer in our lab.

Formation of Λ-doublet states are observed in photoproducts containing diatomic molecules with an unpaired electron such as NO.[67] A Λ-doublet propensity indicates that the

fragment retains stereochemical information about the bond that is broken in dissociation, and it is reflected in the orientation of the orbital relative to the rotation of the diatomic fragment. In the present article, the states are depicted following the notation used by Alexander et al.[68] The two states are denoted by Π(A″) and Π (A′) in which the unpaired electron in the π orbital is either aligned parallel to J or resides in the plane of rotation of the molecule respectively. Spectroscopically, the populations of the two -doublet states can be probed by measuring the relative population through different rotational branches although the actual energy splitting between the states is quite small. The Π(A″) state is sensitive to the Q branch and (A′) state is sensitive to the P (or R) branch.[69]

The orbital alignment for the nascent NO products can also be expressed in terms of degree of electron alignment (DEA) as (Π(A″) − Π(A′))/(Π(A″) + Π(A′)). For a complete orbital alignment of the products, DEA = 1. We can use the REMPI spectrum recorded for nitromethane IRMPD in Fig. 3.2 to obtain the -doublet propensities. The DEA for the products was calculated by integrating the area under the peaks for transitions of Q and R branch from the spectrum. The plot of DEA against J value is shown in Figure 3.7. The plot shows that the DEA value steadily increases from 0.03 to 0.24 with increasing J values. There is a single outlier at J = 12.5 which resulted probably from the intensity fluctuation of the probe laser. This implies that at higher J values, the Π(A″) state is significantly more populated. Therefore, it is evident that the dissociation from CH_3NO_2 via TS1 occurs through a planar framework and post-dissociation, the unpaired electron in the pπ orbital is preferentially aligned parallel to J in the nascent NO fragments.

In contrast to this, careful IRMPD studies on methyl nitrite by King and Stephenson show the absence of a -doublet propensity.[70] Integration of our images in Figs. 3.4 and 3.5

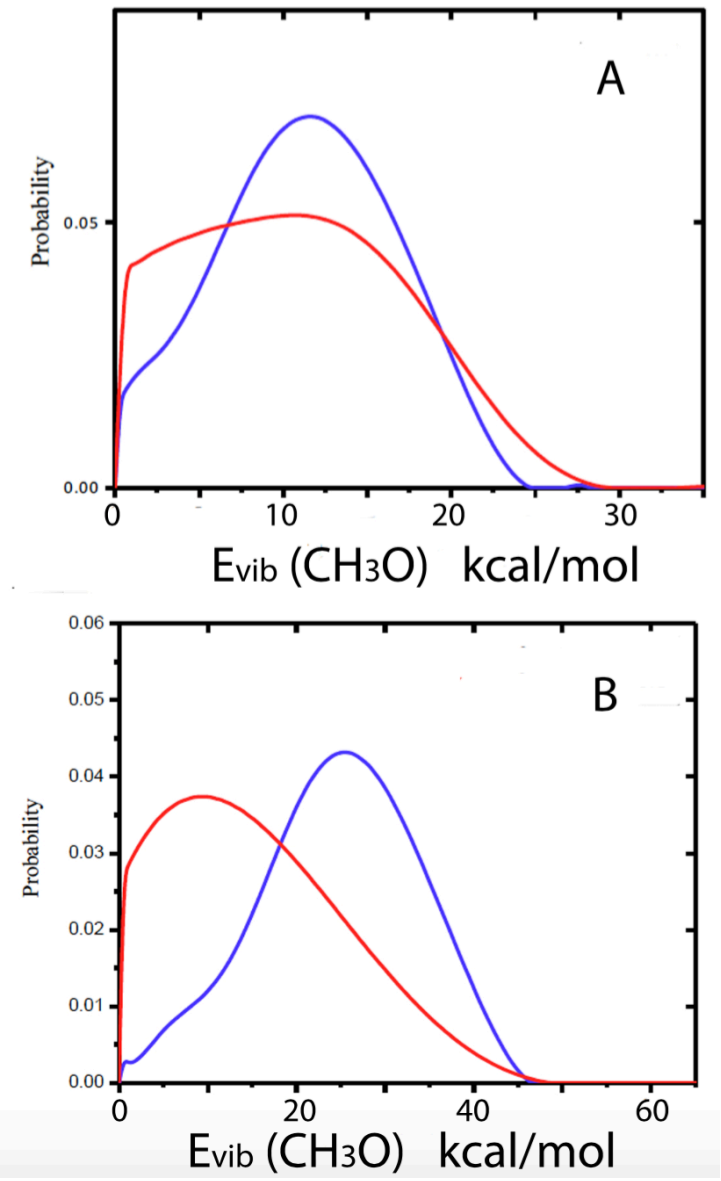

Figure 3.8: Methoxy radical vibrational energy content for trajectories initiated at the nitromethane global minimum (blue curves) or at the *cis*-methyl ni- trite minimum (red curves). (a) Total energy 63 kcal/mol and (b) total energy 89 kcal/mol.

may also be used to explore the -doublet propensities, and these are consistent with the results in Fig. 3.7 and those of King and Stephenson, i.e., a significant Λ -doublet propensity is seen for IRMPD of nitromethane, while none is seen for methyl nitrite IRMPD. Earlier, the UV photodissociation dynamics of methyl nitrite and its -state populations were studied extensively using one-photon[71] or two-photon[72, 73] LIF. These studies established that dissociation

occurs through a planar CONO framework with the unpaired electron preferentially residing in the pπ orbital parallel to J. A remarkable bimodal -doublet propensity was observed in "roaming" mediated dissociation of NO_3 by North and co-workers.[35] In that case, the nascent NO fragment showed opposite alignment of the pπ orbital for dissociation of NO_3 originating from the ground and excited state.

These results suggest two possibilities: the -doublet propensity seen in IRMPD of nitromethane may be a signature of the roaming pathway and the transition state TS1, giving rise to dissociation from restricted geometries and a nonstatistical product state distribution. Alternatively, the difference might simply reflect the different available energies, as IRMPD from nitromethane necessarily occurs at a significantly higher energy relative to the global minimum compared to methyl nitrite. We have examined the vibrational excitation in the methoxy radical product in the trajectory calculations to gain insight into this question. We have initiated these trajectories at two energies starting either at the global minimum (nitromethane) or at cis-methyl nitrite. The results, shown in Fig. 3.8, reveal sharp differences: the methoxy product formed via TS1 shows the substantial vibrational excitation often seen in the new bond in a roaming event, while the methyl nitrite case appears fully statistical. This strongly suggests that the passage over TS1 gives rise to a nonstatistical product state distribution and preserves memory of the CONO plane in the subsequent dissociation, with a corresponding - doublet propensity. A rigorous comparison of methoxy internal excitation to experiment is not possible because the precise experimental excitation energy is not known, nor is the full NO internal state distribution measured here. However, if we make the reasonable assumptions that the dissociation is near threshold and the NO product distribution is primarily in v = 0, then we infer that ~14 kcal/mol is in methoxy internal excitation, and this must largely be vibration owing to

angular momentum constraints. If the excitation is further above threshold then any additional excitation energy must also reside in methoxy internal excitation, so this 14 kcal/mol is a lower bound.

We note at the higher energy a pathway to transCH_3ONO via the tight saddle point[47, 48, 59] (TS3) is classic cally energetically open. Dissociation from trans-CH_3ONO to CH_3O + NO is then possible via the conventional pathway indicated in Figure 3.1. We have not investigated the fraction of trajectories that may produce CH3O + NO via TS3 at the higher energy. However, based on both the lower energy and the "floppiness" of the roaming pathway we expect it to be dominant pathway even at the higher energy. We investigated this by running 2000 trajectories from TS3 at this higher energy and observed that the CH3O vibrational distribution peaks at roughly 20 kcal/mol. This is 10 kcal/mol below the peak in the distribution seen in the lower panel of Figure 3.8 for trajectories initiated at the NM global minimum. Thus, this supports the statement that this tight saddle-point pathway is playing a minor role at this higher energy and further supports the methoxy vibration as a "signature" of the roaming pathway in this case.

3.4 Conclusion

To our knowledge this is the first study to combine IRMPD with state selective ion imaging. This approach can provide useful information about the dynamics of unimolecular reactions near threshold that originate from the ground state, features that are particularly relevant for reactions involving "roaming" pathways. IRMPD imaging studies of nitromethane show very low translational energy release of the photofragments and reiterated the importance of "roaming" pathway in the dissociation of nitromethane. These findings are in good agreement with the QCT calculations[47] and the IRMPD studies of Wodtke et al.[20] From the intensities

of the images and recorded IRMPD REMPI spectrum, we find that the A″ Λ-doublet state is more populated. Considering the dissociation to have a planar geometry, it is observed that post-dissociation the unpaired electron preferably stays in the pπ orbital perpendicular to the plane of rotation. In contrast, dissociation of methyl nitrite does not show any Λ- doublet propensity. Significant differences in the methoxy internal state distributions in QCT calculations for nitromethane and methyl nitrite at the same total energy suggest that the Λ- doublet propensity and the methoxy vibrational excitation are both signatures of the roaming-mediated isomerization, with fairly rapid decomposition following isomerization precluding full intramolecular vibrational energy redistribution.

CHAPTER 4 IMAGING NO ELIMINATION IN THE INFRARED MULTIPHOTON DISSOCIATION OF NITROALKANES AND ALKYL NITRITES.

4.1 Introduction

Roaming-mediated isomerization (RMI) is now a widely recognized pathway in the dissociation of nitro compounds.[39, 45, 47, 48, 66, 74-76] The phrase was introduced in a description of nitrobenzene dissociation[45], but the phenomenon was first recognized earlier, in nitromethane decomposition.[48] In a well-known study of the infrared multiphoton dissociation of nitromethane from Wodtke et al., branching up to 40% to NO elimination was seen, and ascribed to efficient isomerization to the nitrite prior to dissociation.[19, 20] RRKM modeling led them to place the isomerization barrier ~5 kcal/mol below the C N bond fission threshold. For many years theorists failed to confirm this interpretation, as calculated barriers to isomerization were generally found 5–10 kcal/mol above the bond fission threshold, too high to make this a plausible pathway. One multireference calculation did identify a loose transition state at long range that, in retrospect, captured the key features of the RMI [48, 63]. However, it was in a later study by Zhu and Lin, following the recognition of roaming dynamics in formaldehyde, that the nature of RMI in nitromethane was fully appreciated. Multiple roaming steps have been seen in trajectory calculations[46, 47] and numerous roaming pathways have been identified both on the ground state and in excited states.[75, 76] An interesting question is the extent to which the same dynamics are involved in larger molecules where competing pathways may come into play. To gain insight into this question, we here study the NO elimination channel in dissociation of a series of nitroalkanes, contrasting these with the corresponding alkyl nitrites. Infrared multiphoton dissociation (IRMPD) is a powerful technique for studying the ground state dissociation of molecules, as it is analogous to thermal excitation but may be performed under

collisionless conditions so that the primary reaction products may be probed.[19, 20, 77] After dissociation, productfragments can be measured to obtain the velocity distribution and angular distribution, and hence the translational energy distribution of the fragments. IRMPD studies were pursued by a number of groups in the past, and systems of interest included nitroalkanes, halocarbons, and others[18, 21, 78-80] Often, earlier studies employed 'universal' but non-statespecific probes to gain global insight into the reaction mechanisms and pathways.[13, 15, 18-21, 81-83] Complementary information may, however, be obtained from state-resolved detection such as that afforded by ion imaging [49, 50] with resonant multiphoton ionization (REMPI) detection, which has emerged in recent decades as a very powerful means of studying photochemical processes.

4.2 Experimental

A molecular beam containing the sample seeded in helium was introduced to the source chamber with a supersonic expansion from a solenoid pulsed valve (General Valve Series 9) of nozzle diameter 0.8mm. The valve includes a copper nozzle extension that is heated to enhance the multipho- ton dissociation process. The temperature of the nozzle was 350 $^{\circ}$ C for nitromethane, nitroethane, butylnitrite, and t-butylnitrite, and 150 $^{\circ}$ C for nitropropane. The molecular beam was then introduced to the detection chamber through a skimmer of 1 mm diameter. The source chamber pressure was maintained at 1×10^{-5} Torr and the pressure of the detection chamber was maintained at 1×10^{-7} Torr. The molecular beam was crossed by a line-tunable TEA-CO_2 laser beam (GAM EX100/60-CO2) and a 226 nm probe beam after entering the detection chamber. The CO_2 laser line was 10.6 m for n-butylnitrite and t-butylnitrite, 9.6 m for nitroethane and nitro- propane, and 9.56 m for nitrobutane. These were found to give optimum signal levels. The NO (v = 0) fragments produced from the dissociation were then

ionized by 1 + 1 REMPI near 226 nm. We did not investigate possible production of NO (v = 1). The 226 nm beam was produced by mixing the fundamental output of the pulsed dye laser (DCM in ethanol) pumped by the second harmonic of a seeded Nd: Yttrium aluminum garnet (Nd:YAG) laser with the third har- monic of the same Nd:YAG laser. The power of the 226 nm beam was maintained as low as 0.20 mJ/pulse to reduce probe-induced signals, while the power of the CO_2 laser was ~100 mJ/pulse for 10.6 m and ~60 mJ/pulse for 9.6 m and 9.56 m. The two lasers were counter propagating. The CO_2 laser beam was focused using a f = 450 mm ZnSe lens and the 226 nm beam was focused with an f = 380 mm lens. The CO_2 laser was displaced slightly upstream and fired 1.2 s prior to the 226 nm beam. The ions were directed through a 60 cm length time of flight tube and detected using a 120 mm micro channel plate coupled with a phosphor screen. A USB CCD camera (USB 2 uEye SE, IDS) was used to capture images and acquisition was done using our own NuACQ program, building on detection methods developed earlier in our group.[84] The acquired images were analyzed to obtain the total translational energy distributions.

4.3 Results and Discussion

REMPI spectra were recorded for the product NO on the 0-0 band for the $A(^2\Sigma^+) \leftarrow X(^2\Pi_r)$ transition and are shown in Figures 4.1–4.3 for the target molecules of interest. In each case we examine the C2, C3 and C4 systems together and compare the nitrite result to the corresponding nitro compound. The spectra were recorded in the range of 44180–44450 cm^{-1} . The peaks were assigned to each rotational level by comparing them to a simulated NO spectrum obtained using LIFBASE[85] and rotational distributions were extracted from the spectra. The corresponding rotational temperatures were obtained by plotting the density of the rotational

states, $\ln[P(v'',J'')/(2J''+1)]$, against the internal energy, $B_{v''} J''(J''+1)$. The rotational distributions could be described by a combination of two Boltzmann distributions. All spectra had a low-J component showing a rotational temperature below 100 K that we associate with residual NO in the beam. This component is not treated further and images were not recorded on rotational levels below J = 10.5. These Boltzmann plots are given in Figure 4.4. Rotational temperatures obtained for each molecule after fittings are presented along with the plots.

DC sliced images and total translational energy distributions for selected rotational levels following IRMPD are given in Figures 4.5, 4.6 and 4.7 for C2, C3, and C4 systems, respectively. Higher intensities of the image correspond to higher signal strength, and the distance from the center of the image gives a measure of the recoil velocities of the products. Images were recorded for selected J values ranging from 10.5 to 25.5 for $v = 0$. The velocity distributions of the products from IRMPD were obtained from the NO images by direct integration with appropriate weighting. Total translational energy distributions were then calculated from the images using conservation of momentum, and these are given along with the images in Figures 4.5–4.7. The average translational energy release for each system and each rotational level was obtained from the translational energy distribution. These are given for all systems studied and all rotational levels, along with the rotational temperatures, in Figure 4.8. The average translational energy release for nitroethane ranges from 4.9 kcal/mol to 7.0 kcal/mol (low-J to high-J) while for ethyl nitrite it ranges from 1.2 kcal/mol to 1.4 kcal/mol. The limiting value for the total translational energy release of nitroethane was found to be ~14 kcal/mol and ~5 kcal/mol for ethyl nitrite. This difference in the translational energy release is also manifested in the product rotational excitation: 1600K for nitroethane and 768 for ethyl nitrite. We note also

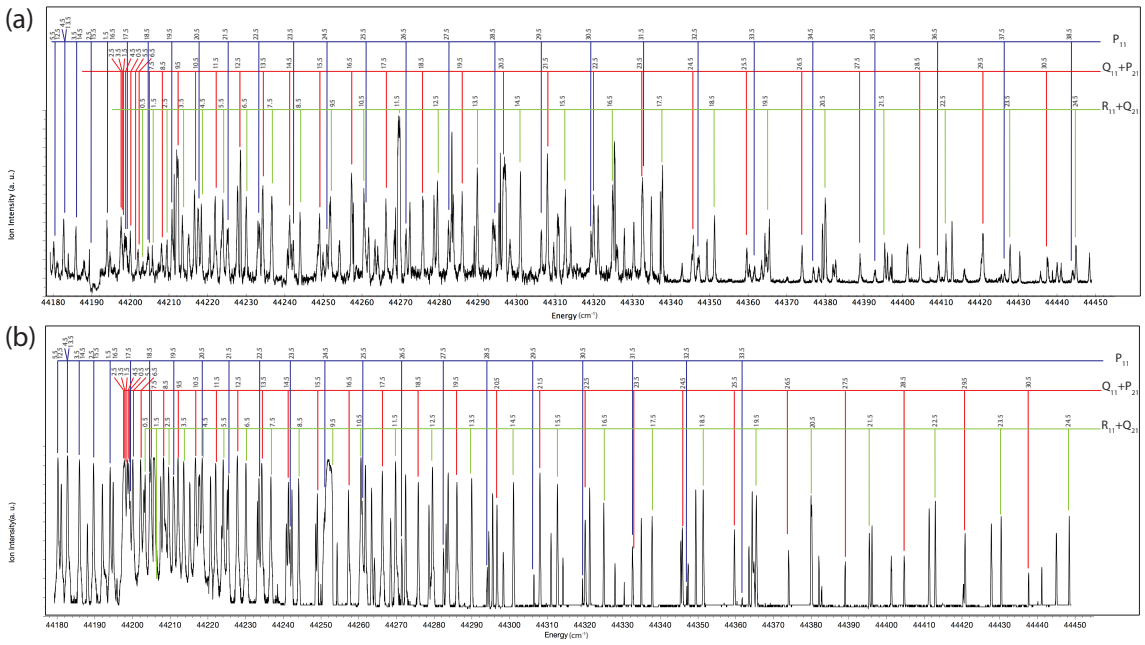

Figure 4.1: REMPI spectrum of nascent NO formed from the IRMPD of nitroethane (a) and ethyl nitrite (b). The peaks are fitted to the rotational lines for the $A(^2\Sigma^+)\leftarrow X(^2\Pi_r)$, v(0,0) transitions acquired from the LIFBASE program.

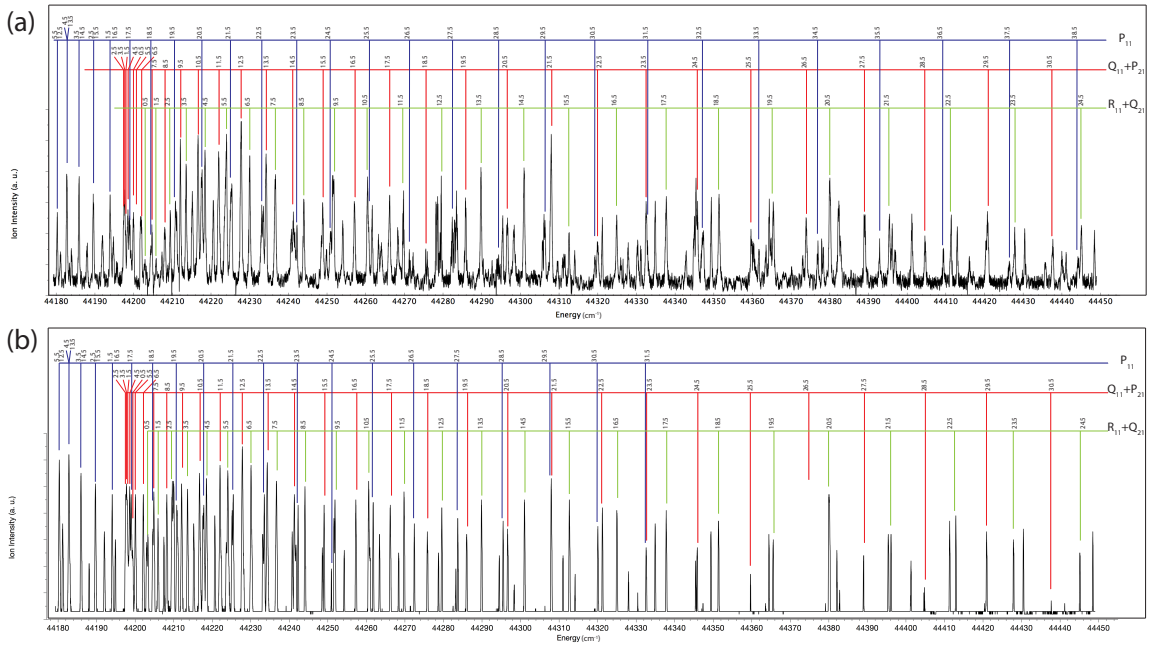

Figure 3.2: REMPI spectrum of nascent NO formed from the IRMPD of nitropropane (a) and propyl nitrite (b). The peaks are fitted to the rotational lines for the $A(^2\Sigma^+)\leftarrow X(^2\Pi_r)$, v(0,0) transitions acquired from the LIFBASE program.

that for nitroethane (and the other nitro systems), there is a correlation between average

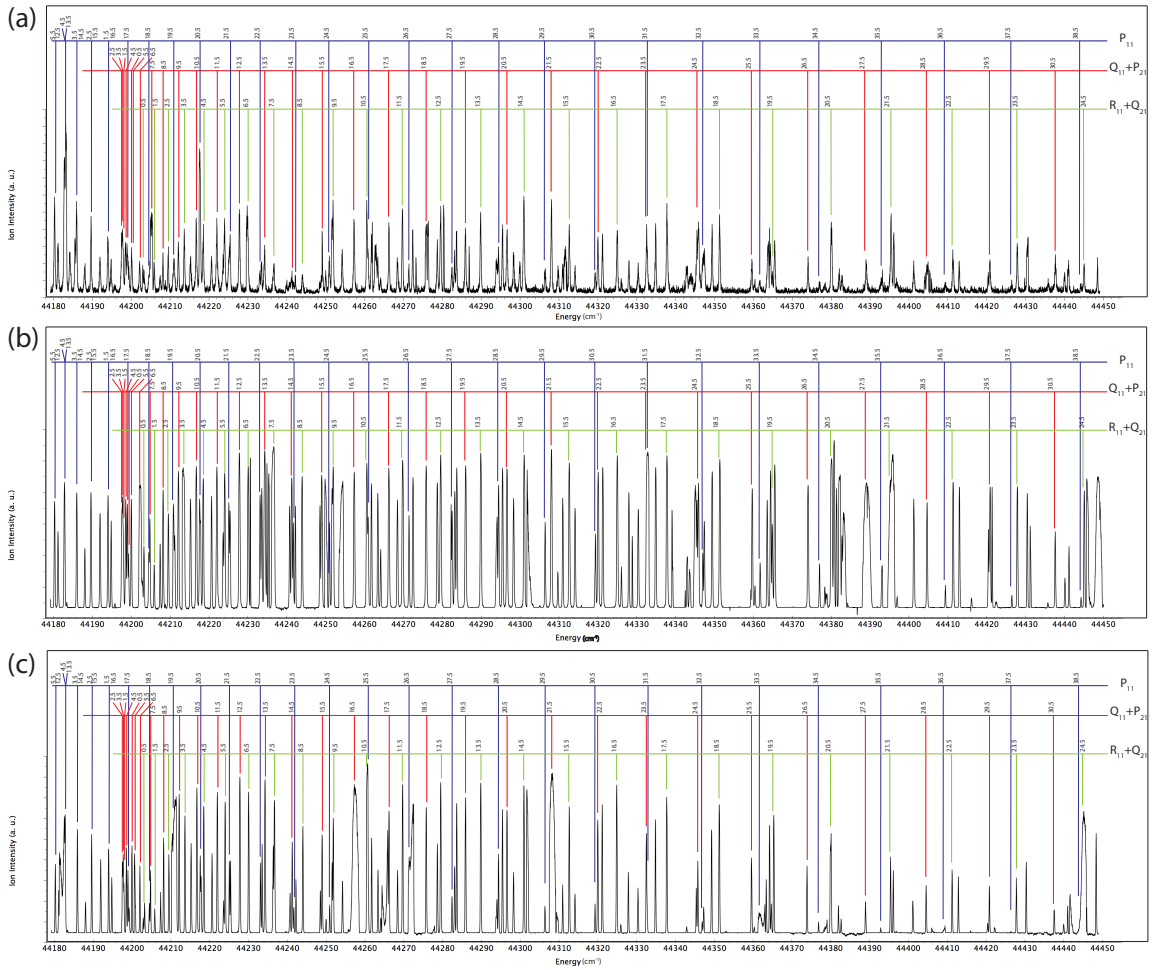

Figure 4.3: REMPI spectrum of nascent NO formed from the IRMPD of nitrobutane (a), butyl nitrite (b) and t-butyl nitrite (c). The peaks are fitted to the rotational lines for the $A(^2\Sigma^+)\leftarrow X(^2\Pi_r)$, v(0,0) transitions acquired from the LIFBASE program.

translational energy release and rotational excitation (Figure 4.8), consistent with an impulsive origin of the rotation. Interestingly, this is not seen for the nitrites. These results show the same trends as the IRMPD results of nitromethane and methyl nitrite we reported previously, supporting the association to RMI.[74] The isomerization of nitroethane to ethyl nitrite has to compete with the direct C-N bond fission channel and an alternative pathway, concerted molecular elimination (CME) to HONO + ethylene, for which there is no analogue in nitromethane. Denis et al. reported a density functional study of the stationary points relevant to decomposition of nitroethane and 2-nitropropane in 2003.[86] They found the barrierless simple

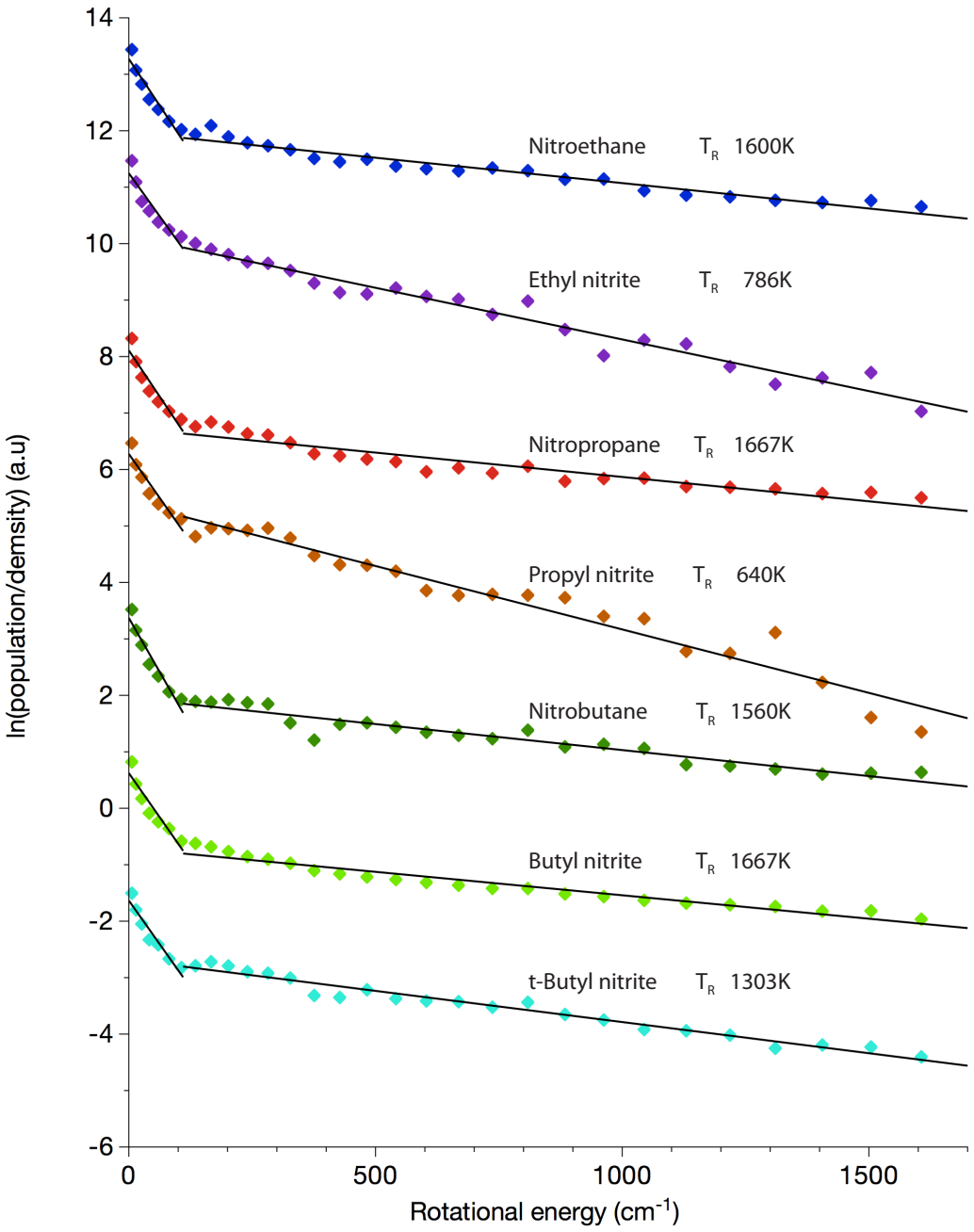

Figure 4.4: Rotational state distribution of NO obtained from IRMPD.

bond fission (SBF) of the C _N bond at 53.8 kcal/mol above the nitroethane minimum, and they placed the TS for CME about 12 kcal/mol lower. They found a tight TS for isomerization to the nitrite 6 kcal/mol above the SBF channel and troubled over this, as they also found a similar value for nitromethane. However, as noted by Lin[48], this high barrier would not permit

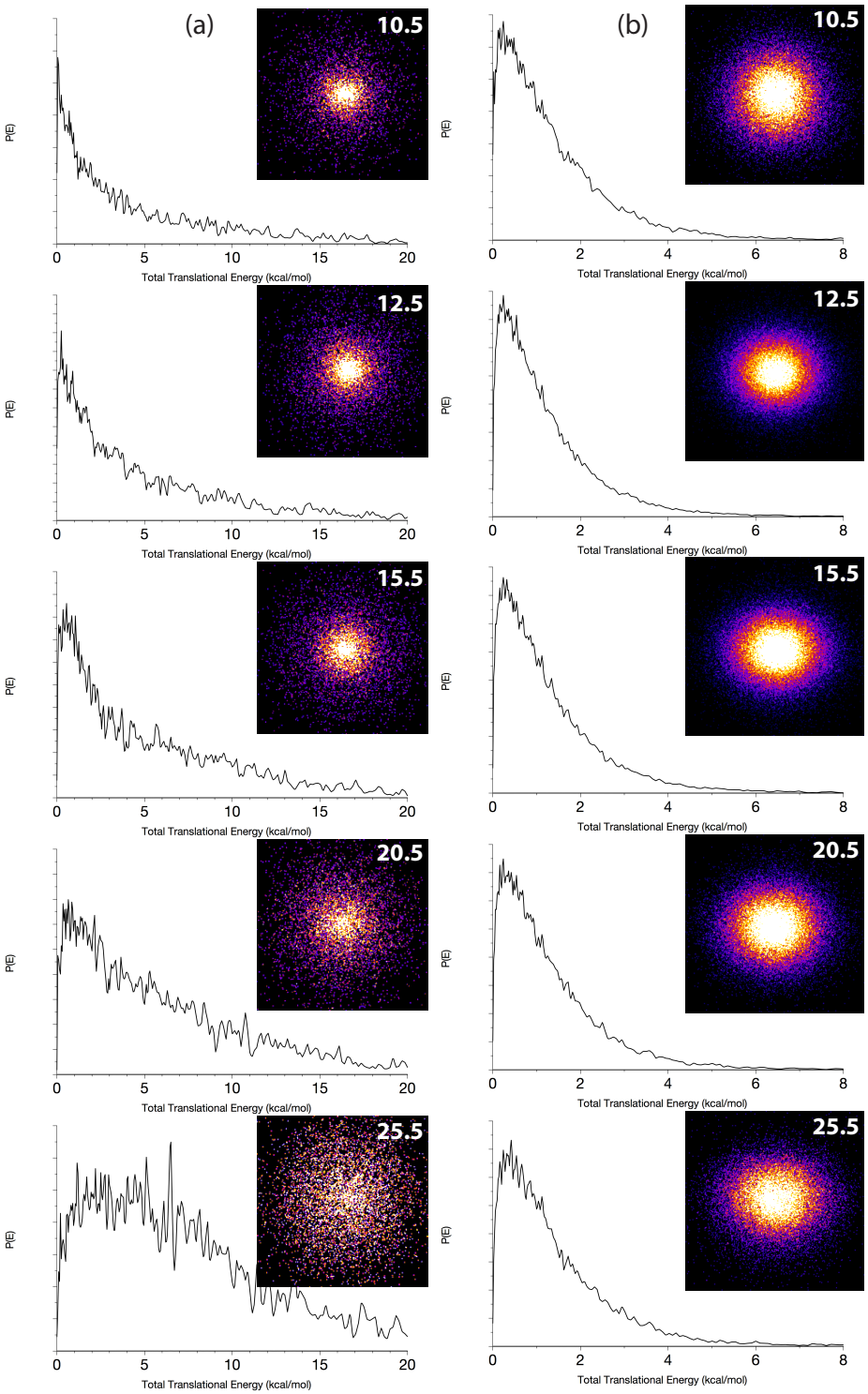

Figure 4.5: Direct current sliced images of NO obtained from IRMPD of nitroethane (a) and ethyl nitrite (b). Nitroethane was dissociated by setting the CO2 laser at 9.6 m and 10.6 m for ethyl nitrite. NO was probed around 226 nm. The images were recorded for different rotational levels in the Q branch. The center-of-mass total translational energies of the fragments are also presented.

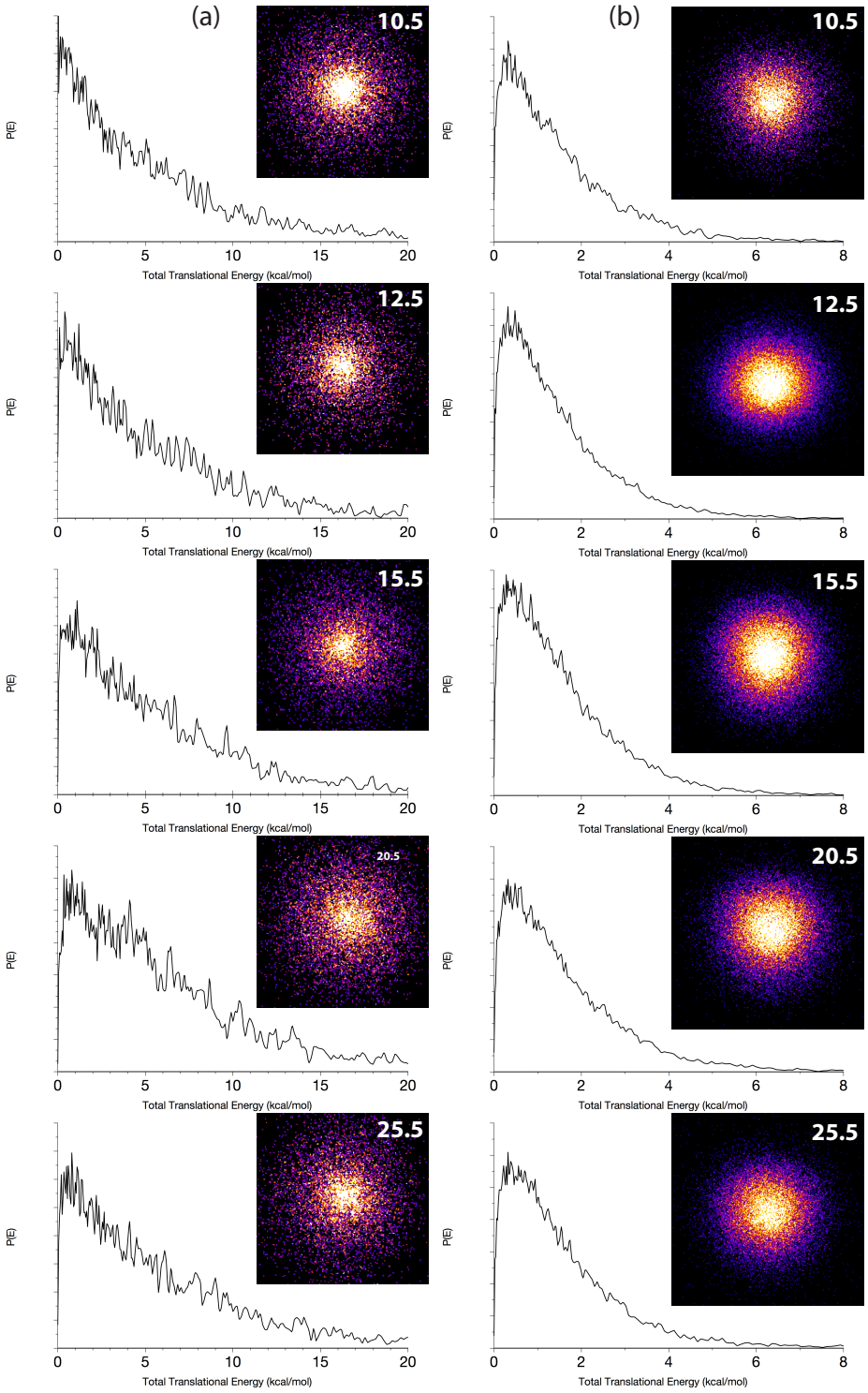

Figure 4.6: Direct current sliced images of NO obtained from IRMPD of nitropropane (a) and propyl nitrite (b). Nitropropane was dissociated by setting the CO2 laser at 9.6 m and 10.6 m for propyl nitrite. NO was probed around 226 nm. The images were recorded for different rotational levels in the Q branch. The center-of-mass total translational energies of the fragments are also presented.

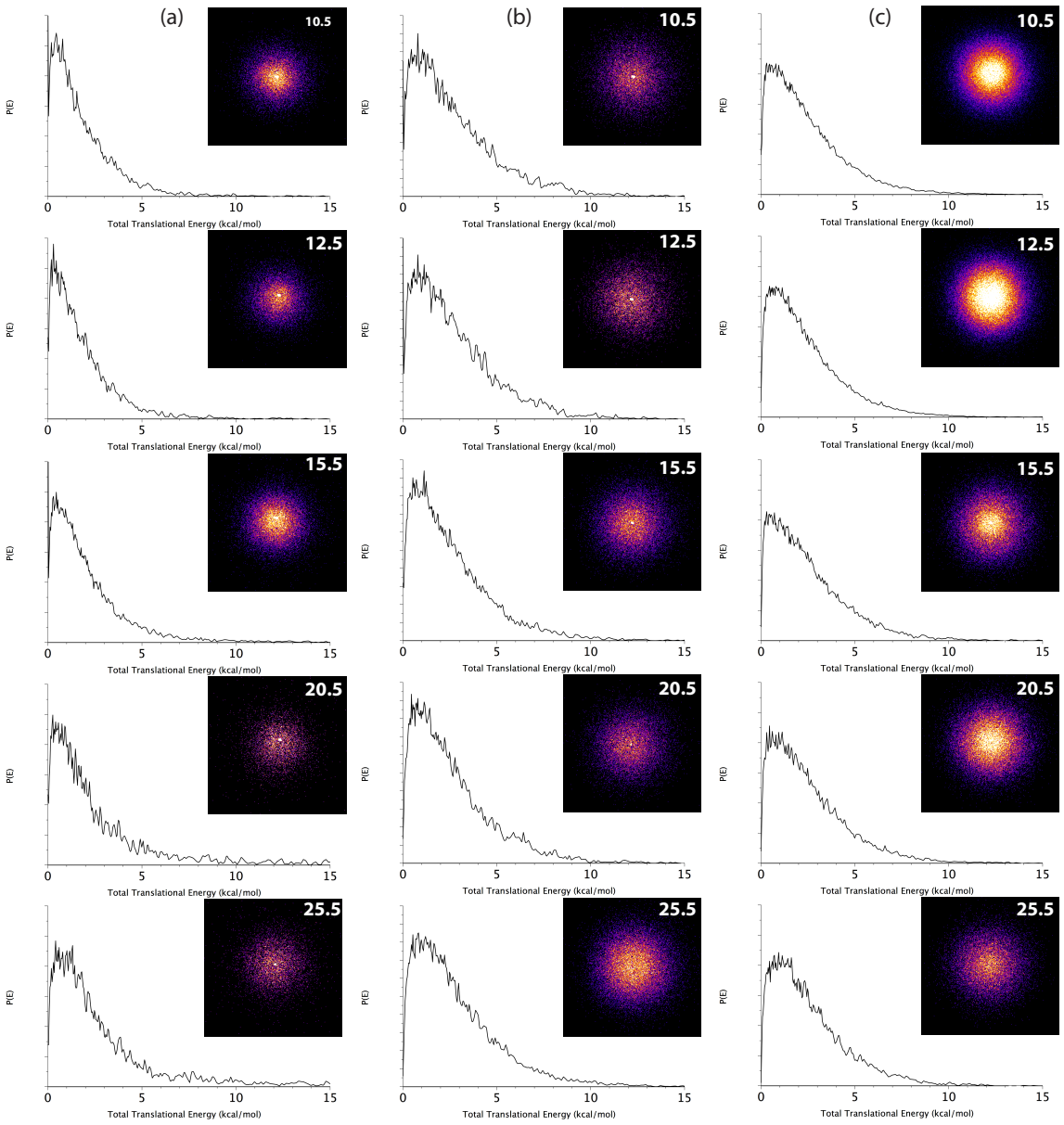

Figure 4.7: Direct current sliced images of NO obtained from IRMPD of nitrobutane (a), butyl nitrite (b) and t-butyl nitrite (c). Nitrobutane was dissociated by setting the CO2 laser at 9.6 m and 10.6 m for butyl nitrite and t-butyl nitrite. NO was probed around 226 nm. The images were recorded for different rotational levels in the Q branch. The center-of-mass total translational energies of the fragments are also presented.

effective competition between isomerization and SBF as had been seen for nitromethane in the Wodtke and Lee experiments[20]. Denis et al.[86] concluded in any case that the CME channel would domi- nate in nitroethane and nitropropane, and took solace in the fact that Wodtke and Lee[19] did not see a measurable yield of NO in the nitroethane case. However, our results

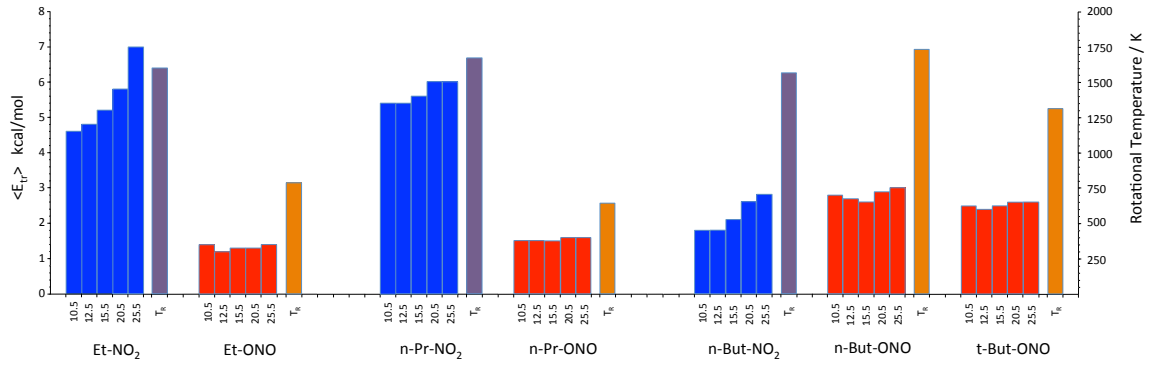

Figure 4.8: Average translational energy release for indicated rotational level (left) and rotational temperature T R (right).

clearly show that isomerization to the nitrite does occur, as this is the only feasible means of producing NO from the nitroethane. Furthermore, the likely mechanism is RMI, just as in the nitromethane case. However, although the branching to isomerization is substantial for nitromethane, our results give no indication as to the branching here: it could be and likely is relatively small. Indeed, Wodtke et al. [19] reported no evidence for isomerization in IRMPD of nitroethane or 2-nitropropane; however they did not report an upper bound for this channel. Given mass spectrometric interference from both NO_2 and HONO at m/z = 30 in their study, and the challenge of identifying ions associated with C_2 H_5 O, it is reasonable to imagine that branching up to 15% could easily be overlooked in those experiments. In any case, our results suggest that there is a loose roaming transition state analogous to that found by Zhu and Lin for the nitromethane case [48], or else isomerization would be very unlikely, as suggested by Denis et al. [86]. Nitroethane and the other systems studied here all have the vicinal carbon that allows for the five-membered transition state leading to CME.[87-89] In a sense, these systems have aspects in common with the formaldehyde potential surface in which roaming was first recognized. In formaldehyde, the SBF threshold and the roaming TS are also above a CME transition state, about 7 kcal/mol higher in that case.[29, 90] The extent to which roaming

persists above the SBF threshold is strongly system-dependent, and a subject of considerable interest. In formaldehyde, branching to the roaming pathway remains significant even at energies 10 kcal/mol or more above the roaming threshold.[90] In the nitrate radical, RMI shuts down almost immediately above threshold. In nitromethane, there is some disagreement among the theoretical treatments. Homay- oon and Bowman used full-dimensional quasiclassical trajectory calculations[47] and saw RMI persist more than 5 kcal/mol above the SBF threshold. Annesley et al. used a reduced dimensionality 'rigid- body' trajectory treatment and concluded that RMI is operative only up to 2 kcal/mol or so above threshold.[76] They also reported the pressure dependence and concluded that SBF will dominate at high pressures (120 Torr). We should note that, following isom- erization to the nitrite, pathways leading to HNO + acetaldehyde are also accessible, either via a four-center transition state, or by NO roaming.[47, 66, 75] A recent report of ethyl nitrite pyrolysis using chirped-pulse mm-Wave spectroscopy and kinetic mod- eling has concluded that roaming dynamics are responsible for HNO formation in that case.[39] Future studies to determine the branching accurately for these systems would be of considerable interest. 1-Nitropropane and propyl nitrite are the next systems we consider. Again, in the NO elimination channel we see behavior reminiscent of nitromethane. 1-Nitropropane shows an aver- age total translational energy of 4.4–6.0kcal/mol while propyl nitrite has an average total translational energy of 1.5–1.6 kcal/mol (Figure 4.8). The limiting total translational energy of nitropropane is ∼15 kcal/mol and ∼7 kcal/mol for propyl nitrite (Figure 4.6). The NO (v = 0) rotational temperatures are 1667 K and 640 K for nitropropane and propyl nitrite, respectively. To the best of our knowledge, there has been no theoretical characterization of the potential surface for 1-nitropropane. Denis and co-workers studied 2-nitropropane using DFT and found strong parallels to nitroethane[86], i.e. SBF is 52.7kcal/mol above the minimum and the CME

channel is 14kcal/mol below this. The calculated isomerization threshold was 3kcal/mol above the SBF asymptote (rather than 6 as in nitroethane), but as we expect RMI to be dominant, this difference is likely not meaningful.

Finally, 1-nitrobutane, n-butyl nitrite and t-butyl nitrite were studied to generalize our understanding further. Here the results are somewhat puzzling. For nitrobutane we find significantly lower translational energy release than any of the other nitro compounds, yet we still observe a correlation between translational energy release and rotational excitation (Figure 4.8). The translational energy release for the two butyl nitrites is some- what greater than the other nitrites but again show no rotational correlation. However, the rotational temperatures obtained for all three C4 systems are rather large, 1300–1700K (Figure 4.4). It is difficult to rationalize these observations. We note that the NO yield for nitrobutane appeared qualitatively to be large, i.e., the signals were very strong in this case unlike nitroethane and nitro- propane. It is also possible that the IR excitation is more efficient for the butyl nitrites, and excitation takes these systems higher above threshold, resulting in larger rotational and translational excitation. Unfortunately there has been no detailed investigation of the potential surface for nitrobutane. In addition to the CME pathway analogous to nitroethane and nitropropane, there may be 6-membered cyclic intermediates that could play a role in the nitrobutane case, providing an efficient alternative path to NO release other than RMI that competes with CME. Additional theoretical input would clearly be valuable to address these questions. We note that we considered the possibility that some of these signals could come from alternative sources such as IRMPD of NO_2, HONO or HNO. However, none of these species have transitions that coincide with the CO_2 laser. In addition, absorption of dozens of additional photons would be required. We conclude that these alternative explanations for the observed signals are unlikely.

Our studies suggest that IRMPD of nitroethane and nitropropane give rise to NO via RMI despite the fact the CME channel has a significantly lower threshold in both cases. Nitrobutane, however, appears distinct, with NO in that case possibly resulting from a 6- membered transition state or some other pathway not available to the C2 and C3 systems. Theoretical characterization of the potential surface for nitrobutane, and future experiments to determine the branching would be valuable to shed additional light on these systems.

CHAPTER 5 VISIBLE/INFRARED DISSOCIATION OF NO_3: ROAMING IN THE DARK OR ROAMING IN THE GROUNG?

5.1 Introduction

The nitrate radical, NO_3, is an extraordinary molecule that has fascinated and challenged chemists for many years.[91, 92] It possesses several low-lying electronically excited states showing complex vibronic interactions accessible via visible excitation.[93-96] Its photochemistry is also quite unusual, with two dissociation channels, NO + O_2 and NO_2 + O, showing nearly the same energy threshold and accessible in the visible,[97-99] giving it an important role in the atmosphere.[100] In hindsight, the close connection between these two reaction channels may be seen as a portent of the recent recognition of the key role of roaming dynamics in this system.[35-37] Roaming is a reaction mechanism in which the molecule undergoes near-dissociation to products, following which reorientation gives access to a distinct intramolecular reactive pathway.[28] It is now recognized as a ubiquitous but long-overlooked mechanism by which molecules decompose.[26, 101, 102]

Roaming in the case of NO_3 is quite unusual, however. Key features of the relevant potential energy surfaces (PESs) are shown in Figure 5.1 to guide this discussion. In recent imaging studies, Grubb et al. [36] found that rotationally selected NO translational energy distributions fell into two distinct groups associated with distinct O_2 vibrational distributions. The low rotational levels were formed with vibrationally excited O_2, while higher rotational levels were associated with vibrationally colder O_2. On the basis of a careful search of the stationary points and the intersections among the relevant PESs, Morokuma and co-workers[38] suggested the following picture of its dissociation dynamics. After optical excitation to the D_3 state (the lower member of the Jahn−Teller distorted E′ pair), the system relaxes via the D_3/D_2

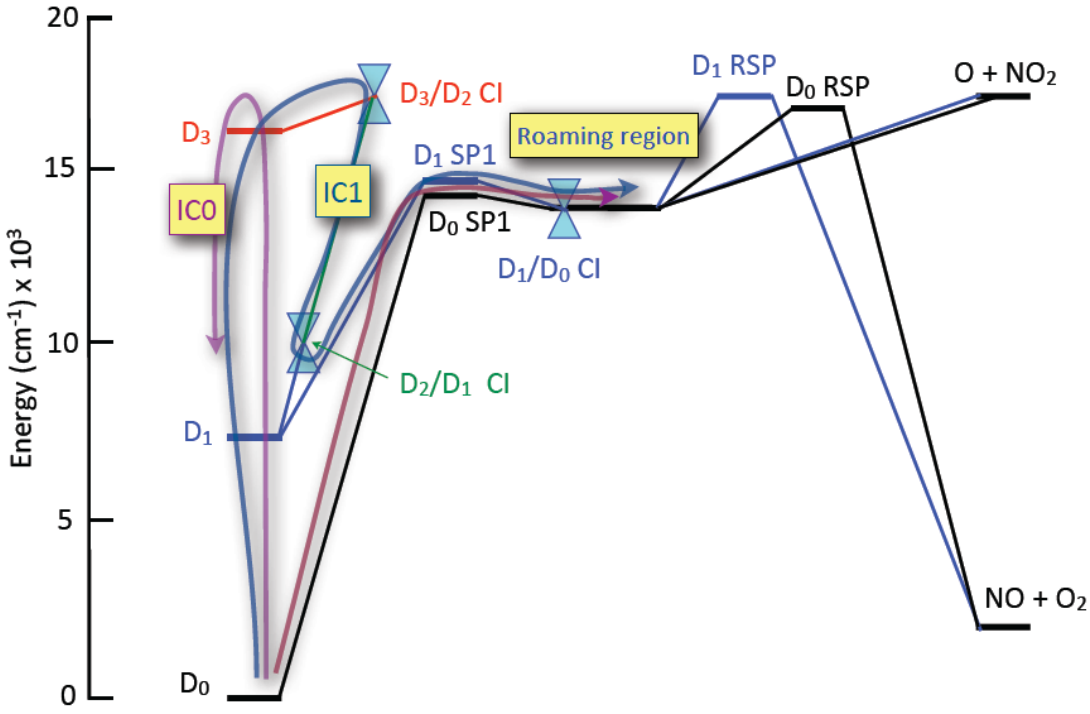

Figure 5.1: Key points on the four lowest adiabatic potential surfaces of NO_3 from Morokuma and co-workers (ref 38). D_0 and D_1 SP1 are saddle points separating the well from the roaming region on the two surfaces, and D_0 and D_1 RSP are RSPs leading to NO + O_2. Minimumenergy CIs are also shown. IC0 schematically portrays direct internal conversion from D_3 to D_0, while IC1 represents the IC pathway that follows the succession of CIs shown.

and D_2/D_1 conical intersections (CIs) to arrive on the dark D_1 state. They argued that the vibrationally colder O_2 product arises from roaming dynamics on D_1 (via the D_1 roaming saddle point (RSP) given in Figure 5.1), while the vibrationally excited O_2 arises via dissociation from the ground electronic state via the D_0 RSP. Strong support for this assignment was seen in the λ doublet propensities, which were found to be opposite and perhaps near-limiting for the two distributions,[35, 103] as well as in subsequent quasiclassical trajectory (QCT) calculations on separate, uncoupled D_0 and D_1 potential surfaces.[104] These remarkable results prompt several questions: What is the branching for dissociation on these two surfaces? What determines this

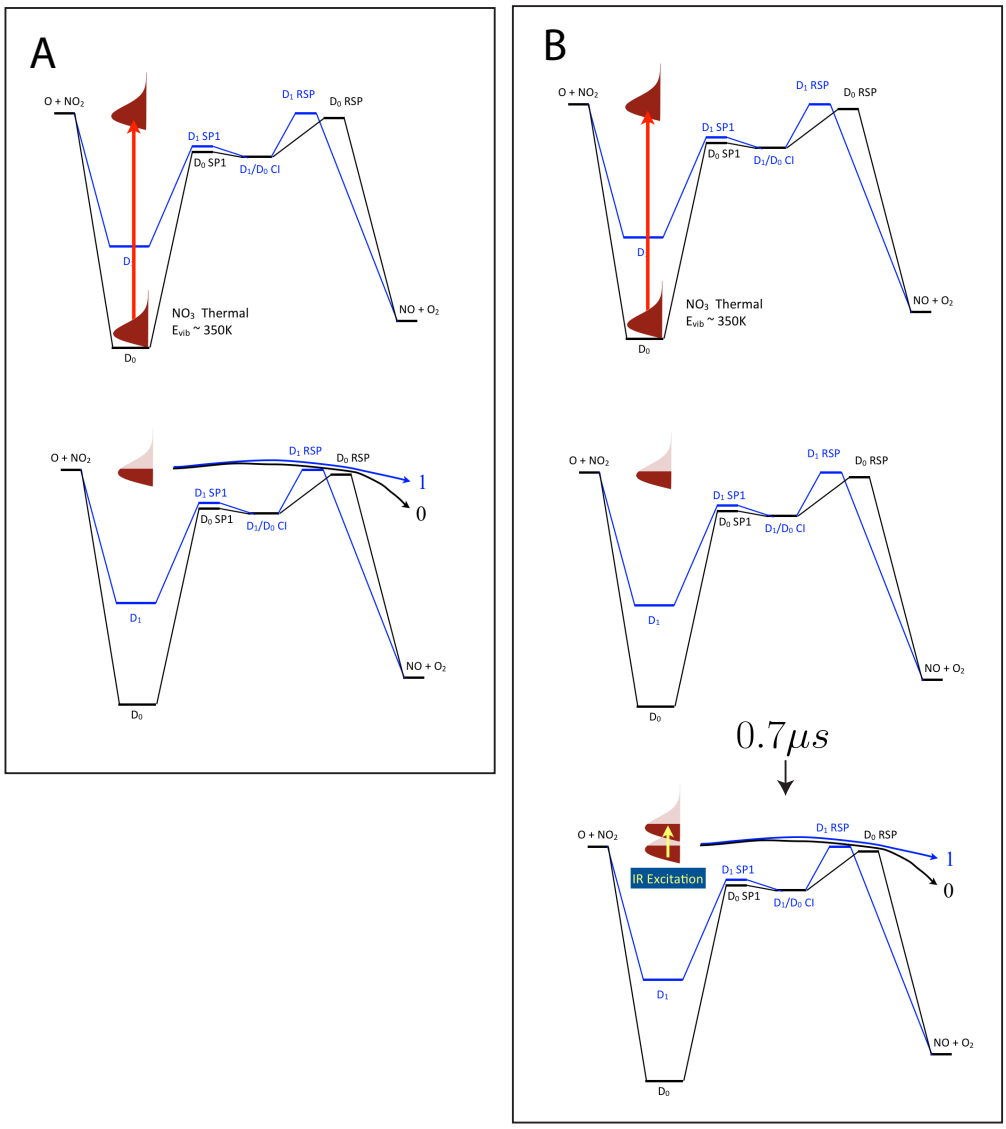

Figure 5.2: Schematic of the experimental approach. (A) Visible excitation of thermal ground state NO_3 leads to prompt dissociation for a subset of the initial population via channels D_1 and D_0. (B) Visible excitation is followed by a 0.7 μs delay, creating a population of NO_3 just below the dissociation threshold. The CO_2 laser pulse then promotes these molecules over the dissociation threshold where they again appear as dissociation products via channels D_1 and D_0.

branching? Does roaming take place exclusively on the dark state or on the ground state, with branching upon exit or on both? Is the branching determined at the intersection between the D_1 and D_0 surfaces in the course of electronic relaxation or possibly from D_0 up to D_1 after an initial relaxation from the bright D_3 state to D_0? To begin addressing these questions, we here

combine state-selected DC slice imaging of the NO product following visible or a combination of visible and infrared excitation from a CO_2 laser, along with additional QCT calculations.

5.2 Experimental

N_2O_5 was used as the precursor for NO_3. The N_2O_5 product was placed in an ice bath, and He (800 Torr) was sent through to prepare the gas mixture. NO_3 was produced by pyrolysis of N_2O_5 at 350 °C using a resistively heated extension tube on a solenoid operated pulsed valve. The NO_3 molecular beam was skimmed and then intersected with three laser beams, 622.9 nm, 226 nm, and 10.6 μm. The 622.9 nm beam was generated from the fundamental output of a pulsed dye laser (Sirah, DCM in ethanol) pumped by the second harmonic of a Nd:YAG laser. The 226 nm beam was generated by mixing the third harmonic of an injection-seeded Nd:YAG laser with the fundamental output of a pulsed dye laser (Sirah, DCM in ethanol) pumped by the second harmonic of the same Nd:YAG laser. The IR beam, 10.6 μm, was produced by a grating-tuned TEA-CO_2 laser (GAM laser). The power of the 622.9 nm beam was ~3.0 mJ/pulse, that of the 226 nm beam was ~0.05 mJ/pulse, and the IR was ~100 mJ/ pulse. The 622.9 nm beam was ~2 mm upstream relative to the 226 nm beam for the two-color photolysis experiments. The 226 nm beam and IR beams were counter propagating. The 622.9 nm was 700 ns prior to the 226 nm, and the IR beam was 250 ns prior to the 226 nm beam. The ions originating from the beams were accelerated through a time-of-flight tube toward a 120 mm microchannel plate detector coupled with a P-47 phosphor screen. A USB CCD camera was used to capture the ion images, and the acquisition was done using our own NuACQ program. The acquired images were used to obtain the total translational energy distributions. The NO probe wavelengths were monitored using a wavemeter and assigned using the LIFBASE program[85] to well-isolated levels of the indicated

rotational branches.

5.3 Computational

The ab initio global PESs of the ground (D_0) and the first excited (D_1) electronic states for photodissociation of NO_3 were calculated based on roughly 90 000 MS-CAS(17e,13o)PT2/aug-cc-pVTZ calculations of electronic energies,[38] using the permutationally invariant polynomial fitting method.[105, 106] Standard QCT calculations were performed on the fitted PESs to get detailed dynamics information on NO + O_2 products. Roughly 400000 trajectories were run initiated from the RSPs of D_0 and D_1 with initial conditions generated using microcanonical random sampling of the initial kinetic energy and with the constraint of zero total angular momentum, respectively. The trajectories were propagated with the time step of 0.12 fs using the velocity Verlet integrator. Most of the trajectories were propagated for a maximum of 20000 time steps (~2 ps), indicating fairly prompt, direct dynamics from D_0 and D_1 RSPs. The trajectories were terminated when one of the internuclear distances became larger than 14 bohr. For those trajectories resulting in NO + O_2 products, the ZPE (zero-point energy) constrained analysis is employed for those trajectories in which NO and O_2 products have at least the corresponding ZPEs.[104] Trajectories that violate the ZPE were discarded. Furthermore, additional trajectories were initiated on D_1 to investigate the energy gaps between the D_1 and D_0 PESs. The ground vibronic state Wigner distribution is typically used to select the initial conditions on the excited- state potential, here D_1.

Densities of states of global minima of D_0 and D_1 (DO-GM and D1-GM) are calculated using the semiclassical approach. Harmonic frequencies and ZPEs of DO-GM and D1-GM are

calculated using the D_0 and D_1 PESs, respectively.[103] Results are given in the next section.

5.4 Results and Discussion

Ideally, to probe the question whether roaming takes place exclusively on the excited state or the ground state, one might contrast dissociation following electronic excitation with that arising from infrared multiphoton excitation. Unfortunately, NO_3 has no infrared-active bands that overlap the CO_2 laser lines; therefore, direct CO_2 laser excitation is not readily achieved. However, several of the unusual properties of NO_3 allow us to begin an investigation along these lines using state- selected DC slice imaging as in the earlier experiments but contrasting pure electronic excitation with a combination of electronic and infrared excitation. This approach is summarized in Figure 5.2. NO_3 is produced in a molecular beam by flash pyrolysis of N_2O_5 at ~350 °C, yielding a beam that is rotationally cold but with a broad vibrational distribution. Visible excitation at 623 nm excites the molecules initially to D_3. As shown by Davis et al., this excitation energy is below the dissociation threshold at 0 K, but even at 300 K, the quantum yield for the NO + O_2 channel at 623 nm is ~15% (with the remaining 85% decaying by fluorescence).[99] Prompt dissociation (i.e., within the 10 ns probe time) of that "hot band" population that exceeds the dissociation threshold gives rise to NO + O_2, which is probed using DC slice imaging[54] of state-selected NO molecules (Figure 5.2A), although a large fraction of the electronically excited molecules do not have sufficient energy to dissociate. This allows us to study the dissociation just at threshold. In a separate experiment, schematically illustrated in

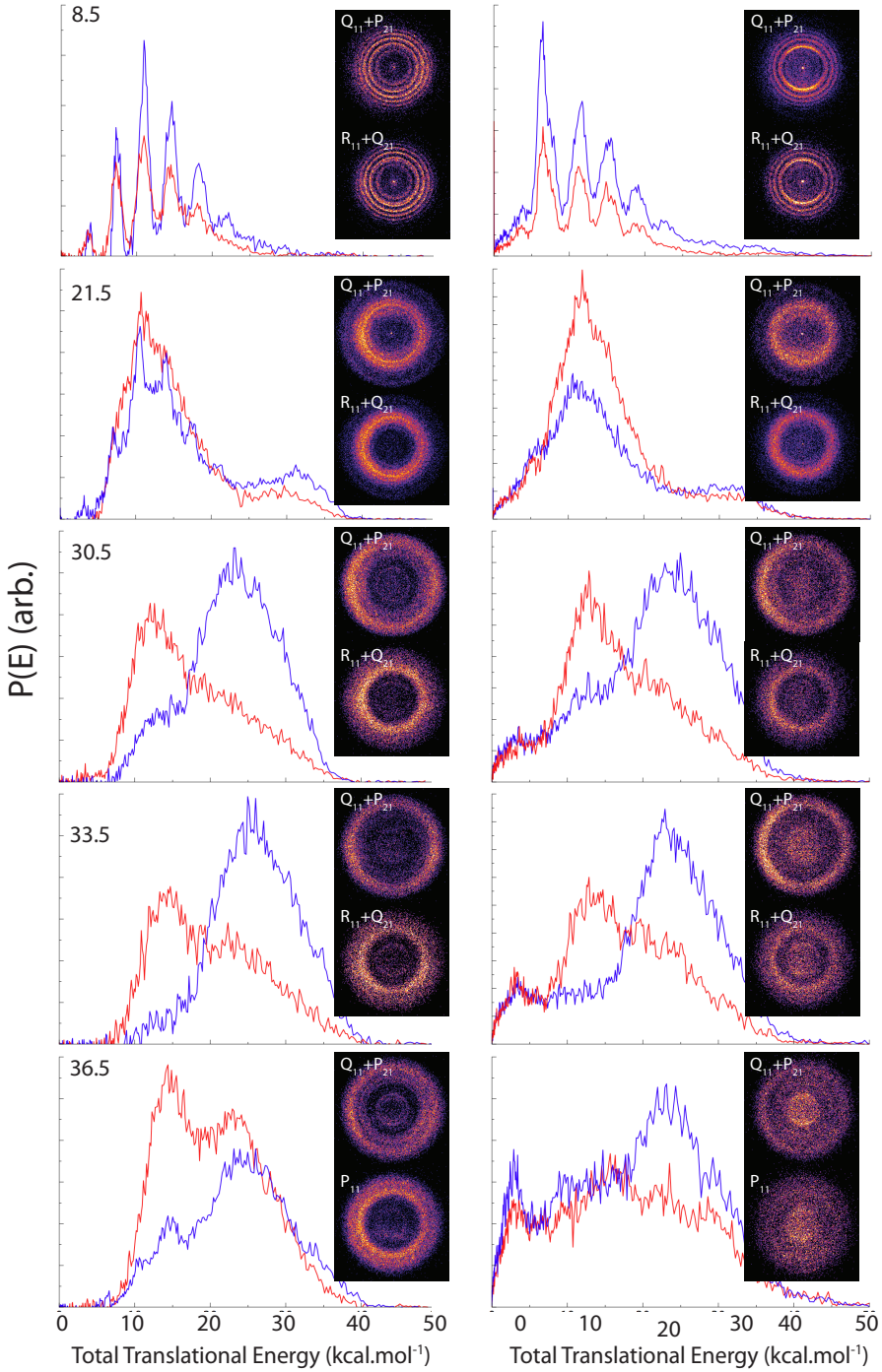

Figure 4.3: NO(v=0, J) DC slice images and total translational energy distributions for visible + IR dissociation (left) or pure visible dissociation (right) for the indicated rotational level and probe transition. Curves in blue are for Q main branch detection, and those in red are for R or P main branch detection. The visible data show a minor contribution from the background from dissociation by the probe laser at lower translational energies that has not been subtracted.

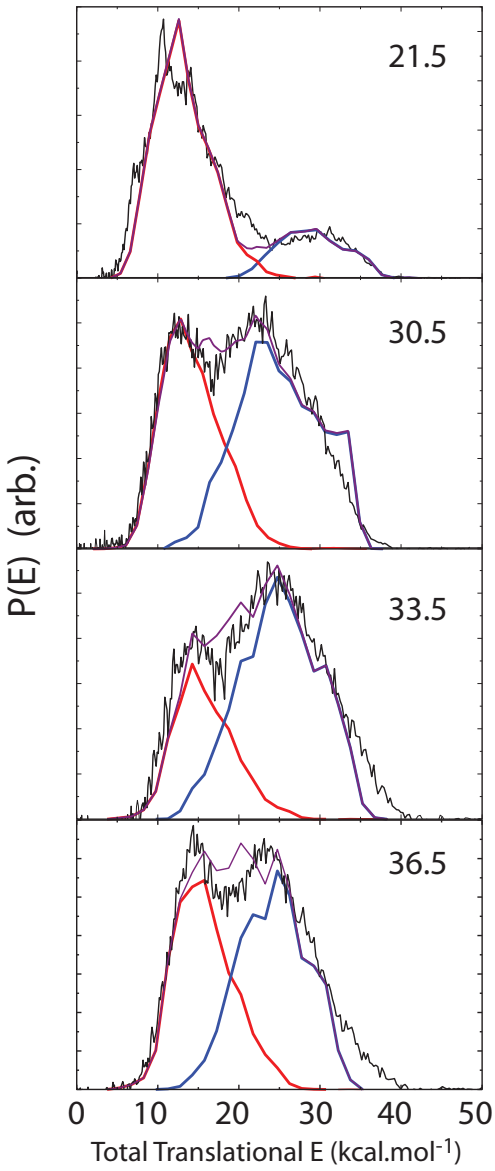

Figure 5.4: Composite translational energy distributions for indicated NO rotational levels obtained by weighting the Q and R,P probe data from Figure 2 by the appropriate line strength factors and then summing them. The composite distributions were then fitted using the separate D_0 and D_1 contributions obtained from the QCT calculations (red and blue curves, respectively). The translational energy for the D_0 components for J = 21.5 and 30.5 was scaled by 80 and 95%, respectively, to obtain accurate fits; otherwise, only the amplitudes were adjusted.

Figure 5.2B, NO_3 is optically excited 1−2 mm upstream of the interaction region. The prompt dissociation is allowed to occur, and then 0.7 μs later, after electronic relaxation, an intense IR laser pulse at 10.6 μm further excites the undissociated molecules over the dissociation threshold.

This delay is chosen to maximize the signal when the electronic excitation is moved upstream as far as is practical. Again, state-resolved slice imaging of the NO product is performed. This allows us to distinguish any dissociation that occurs during the initial electronic relaxation from the long-time behavior of the system. These results are then compared to QCT calculations on the uncoupled surfaces in order to estimate the branching for dissociation on D_0 or D_1.

We performed the two distinct experiments described above, and for each rotational level, we obtained images on P or R branches and on Q branches following the strategy of North and co-workers.[35] Given the large λ doublet propensities seen and the distinct behavior for dissociation on the two surfaces, this is necessary both to aid in assigning clearly the D_0 and D_1 contributions to the dissociation and to determine the branching. The images for visible and visible/IR dissociation are shown in Figure 5.3 for the indicated NO rotational level and the rotational branch of NO used in the probe. As may readily be seen, there are profound differences for Q branch detection as opposed to detection via P,R branches, and this is consistent with the North results. The Q branch probe appears to favor the higher rotational levels that were associated with the D_1 dissociation by Morokuma,[38, 107] while the P,R probe appears dominant for the lower rotational levels that show clear vibrational structure and high vibrational excitation for the O_2 co-product in some cases. This sharply structured low-J component was assigned to dissociation on the ground electronic state, and this was confirmed in the QCT calculations.[104]

We obtained the total translational energy distributions (P(E)'s) from the images, and these are given in Figure 5.3 as well. Although we see distinct differences for each probed rotational level and detection pathway, the results for prompt dissociation with purely electronic excitation shown on the right of Figure 5.3 show little difference when compared to dissociation

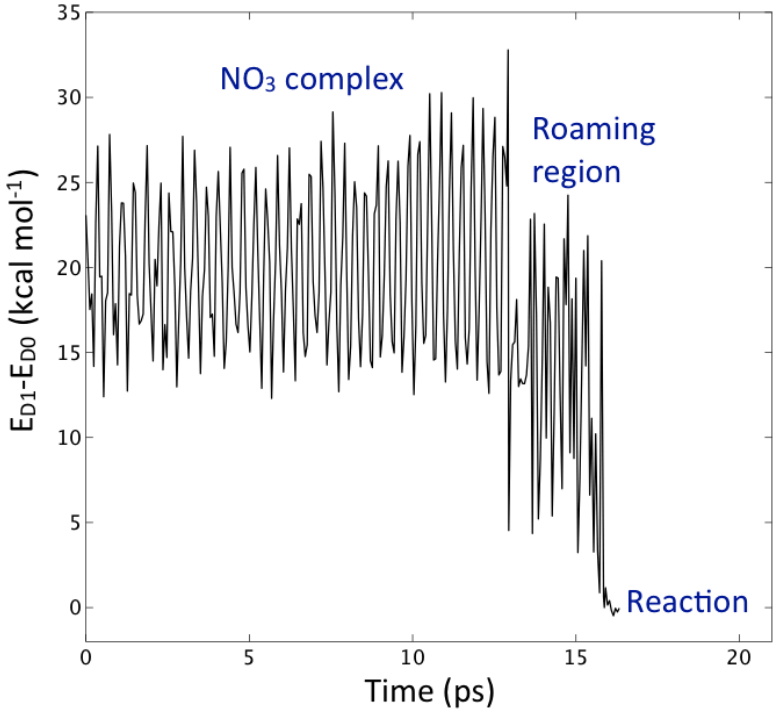

Figure 5.5: Energy splitting between D0 and D1 during the course of a typical trajectory. This trajectory was initiated at the D0 GM with microcanonical sampling of the initial momenta for total angular momentum J = 0.

with a combination of visible and infrared after a 0.7 μs delay. Before discussing the implications of this observation, we first obtain an estimate of the branching between the two dissociation paths based on the measured distributions. Our strategy here is first to create composite translational energy distributions by weighting the distributions in Figure 5.3 using the appropriate line strength factors[108] and then fitting the composite distribution with separate D_0 and D_1 components obtained from the QCT calculations. The results are shown in Figure 5.4. The agreement is generally satisfactory. The relative yields for D_0/D_1 from the fits were found to be 0.92, 0.49, 0.31, and 0.44 for rotational levels 21.5, 30.5, 33.5, and 36.5, respectively. Lower rotational levels are associated exclusively with D_0. This state-dependent branching was then used, with linear interpolation over the rotational distributions given by Wittig and co-workers,[98] to obtain a final branching for dissociation of 6:1 D_0/D_1. This analysis neglects the

minor v = 1 contribution, which has been found to favor D_0 dissociation,[13] as well as rotational levels above J = 40.5, which were not reported by Wittig but are likely to represent a minor contribution. This is largely consistent with the determination of North and co-workers[103] and with the overall translational energy distributions reported by Davis and Lee,[97] although we note that even in our raw images, we see a greater contribution of the slow component than was seen by North and co-workers. It may be that our excitation, which is at somewhat lower energy than in previous photodissociation studies and just above the dissociation threshold, actually gives rise to some greater discrimination between the energies of the RSPs on D_0 and D_1. We plan further experiments to address this question. We now turn to a consideration of the electronic relaxation and dissociation dynamics. The main possibilities, highlighted in Figure 5.1, include initial excitation to the D_3 bright state followed by internal conversion (IC1) through D_2 and D_1 to D_0 via the CIs that were found by Morokuma and co-workers.[104] This pathway is shown as "IC1" in Figure 5.1. The branching for dissociation along D_1 or D_0 that we measure may then reflect the branching at the D_1/D_0 CI as it is encountered during the relaxation. This is the pathway implicit in the treatment of Grubb et al.[35] Alternatively, excitation to the bright state may be followed by IC to the ground state directly from D_3, shown as "IC0" on Figure 5.1. The distinction here is that we recognize that D_3 and D_0 are directly vibronically coupled;[94] therefore, the ground state need not be accessed primarily via D_1 in the roaming region. In this scenario, after IC to D_0, the system may proceed to the roaming region and then "roam upstairs" via the D_0/D_1 CI, which is located in the roaming region. From there, it may roam on D_1 or simply dissociate. If the energy is above the O atom loss threshold, decay via that path is strongly preferred both for D_1 and D_0, based on both experiment[97] and the trajectory

calculations.[104]

One significant feature of NO_3 photophysics impacts this discussion. In the visible region, it is an example of the "Douglas effect," with an anomalously long fluorescence lifetime following excitation to the D_3 state.[105] This is ascribed to mixing of the bright D_3 state with the dense manifold of D_0 and possibly D_1 levels in which it is embedded.[27] Its "long-time limit" thus includes an admixture of the D_3 state with D_0. Indeed, at 0.7 μs, we may be in a fully statistical mixture of the accessible electronic states. This is supported by our calculations of the harmonic vibrational density of states using. At 16200 cm^{-1}, which is roughly the D_3 origin, we obtain state densities of 133 and 17 per cm^{-1}, or a ratio of 8.4:1, which is reasonably close to the experimental branching estimate of 6:1. This density of states ratio would be the RRKM statistical approximation for the experimental branching ratio if the roaming bottlenecks N(E)'s on D_1 and D_0 are the same. Clearly, they are not identical, and if the slightly higher energy of RS1 relative to RS0 is a good indicator of the N(E)'s, then indeed the branching would be slightly less than 8.4:1 and thus closer to experiment. As suggestive as this is, one should take this analysis with a great deal of caution.

Taking all of these points into consideration, we believe that the evidence supports the second alternative relaxation pathway mentioned above, that is, direct IC from the bright state to D_0, with D_1 subsequently accessed from the ground state, probably via mixing in the roaming region where these surfaces are strongly coupled, as shown in Figure 5.5. The points in support of this view are as follows: The D and D surfaces possess 30 strong vibronic coupling, directly impacting both the ground- state vibrational level structure and the bright-state fluorescence lifetimes, while that between the bright state and D_1 is very weak. Moreover, the fluorescence

lifetimes suggest a dilution of the bright state that can only be accounted for by the ground-state density of states.[106, 109] The fact that our translational energy distributions are essentially identical whether we use electronic excitation with a probe on a 10 ns time scale or one coupled with IR excitation 0.7 μs later suggests that this relaxation is complete on the 10 ns time scale.

One other suggestive point from Morokuma's calculations is that the D_3/D_2 minimum-energy CI is at 200.8 kJ/mol, which is nominally above the energy window that gives O_2 + NO and in the region where the branching to NO_2 + O is dominant. It is interesting to speculate whether this is a coincidence or not; perhaps the branching to the atomic elimination channel grows quickly because of the direct access to D_1 that arises via the succession of CIs just as that channel is opened. The QC trajectories from the D_1 global minimum branched more to the atomic elimination than did those on D_0 at the same total energy, providing some support for this picture.[104] In any case, efficient access to D_1 from D_2 seems implausible under our experimental conditions if this location of the D_2/D_1 minimum- energy CI is correct. Although the notion of traversing the D_0/ D_1 CI in the upward direction[110] ("upfunneling") might seem less likely as flux is typically directed away from a CI upon approach from below, because the surfaces are relatively flat and parallel in this region, this view may not be relevant. This aspect of the dynamics is highlighted in the trajectory shown in Figure 5.5. This plot shows the energy splitting between the D_1 surface and the D_0 surface during the course of a typical trajectory. In the complex region, the D_1-D_0 gap is roughly constant at around 20 kcal/mol. When the system reaches the "roaming region", this gap drops to ~13 kcal/mol and remains there until reaction occurs (to O + NO_2 in this case) and the surfaces become asymptotically degenerate. This clearly highlights the interaction between D_0 and D_1 in the roaming region, suggesting the ease in

which D_1 may be accessed from the ground state there.

The final piece of evidence in support of this picture is the branching for dissociation on D_0 and D_1, both in that it strongly favors D_0 dissociation and is insensitive to the nature of the excitation even after a 0.7 μs delay. Although the present results are not yet definitive, in the future, with coupled D_1 and D_0 surfaces, we should be able to probe these questions theoretically by comparing the D_1 and D_0 branching starting from either surface initially. This effort is underway.

CHAPTER 6 DOES INFRARED MULTIPHOTON DISSOCIATION OF VINYL CHLORIDE YIELD COLD VINYLIDENE?

6.1 Introduction

Vinylidene, H_2CC, is a key reaction intermediate and an important initially formed product in many photochemical reactions.[111-113] Perhaps the most frequently cited example, which provides spectroscopic proof that vinylidene is formed, is the vibrationally resolved $H_2C_2^-$ negative-ion photoelectron spectrum.[114, 115] The line widths in this spectrum are widely cited as showing that the isomerization lifetime of vinylidene in its zero-point vibrational level is ~400 fs. Coulomb Explosion Imaging (CEI) experiments[116] of neutral vinylidene 3.5 μs after anion photodetachment showed that roughly 50% of the observed structures are vinylidene-like and 50% acetylene-like. This proves that the vinylidene structure "lives" for at least 3.5 μs. How can this observation be reconciled with a 400 fs isomerization lifetime? The infrared multiphoton dissociation (IRMPD) experiment reported here is undertaken to resolve this paradox and to demonstrate the production of "stable" vinylidene. The resolution of the paradox will emerge as we recall that eigenstates are stationary. The issue is whether one can produce C_2H_2 eigenstates that are predominantly vinyl- idene in character. Such eigenstates were shown to exist in the first full-dimensional quantum calculations by Zou and Bowman,[117] and seen consistently in potential energy surfaces of ever-increasing accuracy since then.[118-120] However, one key to success in experimental production of these eigenstates is that the vinylidene be rotationally cold, as rotation has been shown to promote intramolecular vibrational relaxation (IVR), which profoundly increases the density of acetylene vibrational states into which vinylidene can isomerize.[121, 122] The goal of our IRMPD

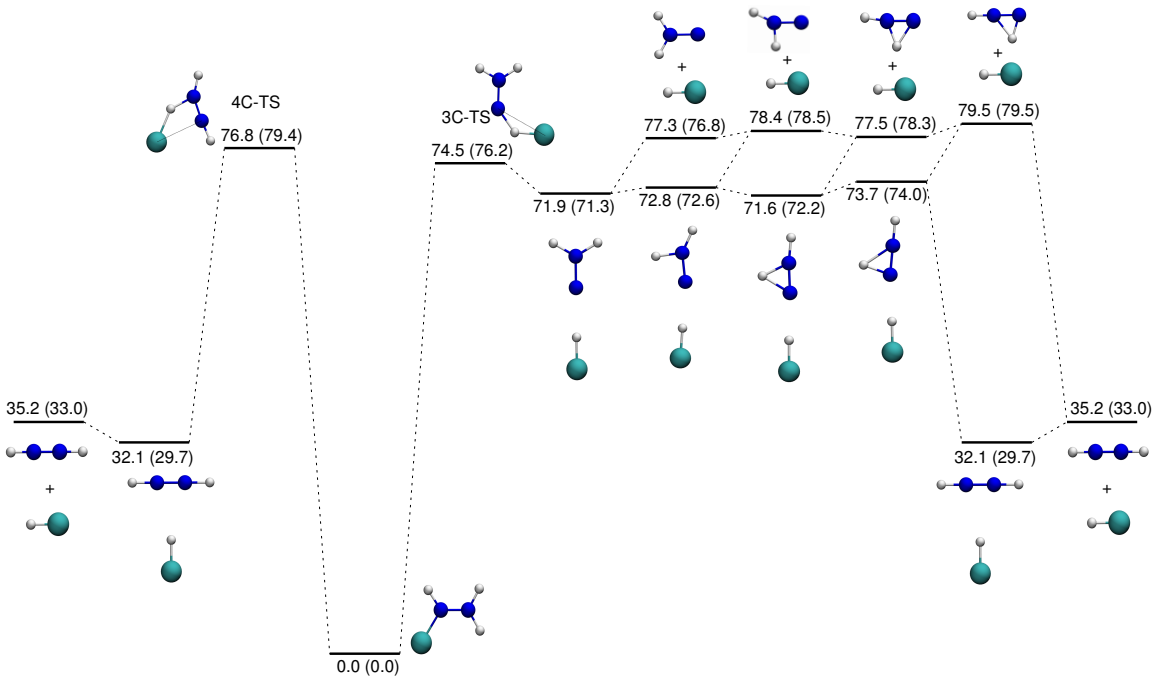

Figure 6.1: Energies (kcal/mol) of stationary points on the vinyl chloride potential energy surface relevant to HCl elimination from DFT-M06-2X/ aug-cc-pVDZ calculations and from CCSD(T)-F12/aug-cc-pVDZ given in parentheses.

experiment is thus to produce vinylidene with only modest nascent rotational excitation, with the expectation that the isomerization dynamics will be encoded in a vastly reduced number of eigenstates. In this Letter we show that IRMPD of vinyl chloride gives rise to HCl in low rotational levels with low translational energy release, consistent with three-center elimination and concomitant formation of rotationally and translationally cold vinylidene.

Photodissociation of vinyl chloride has been studied extensively at 193 nm using a broad range of techniques, which include resonant ionization detection of HCl,[123-125] time-resolved Fourier transform infrared (FTIR),[126] and photofragment translational spectroscopy with vacuum ultraviolet photoionization product detection.[127] Theoretical work has included a detailed mapping of the stationary points on the ground state potential energy surface by Riehl and Morokuma[128] and direct dynamics studies[129, 130] by Martinez-Nunez et al. For HCl elimination, which is the lowest energy decay path and the focus here, there are two reaction

channels as depicted in Figure 6.1: via a three-center (3C) transition state (3C-TS) to HCl + vinylidene, with a zero-point corrected reverse barrier of 2.5 kcal/mol, or by a 4-center (4C)-TS that is 52 kcal/mol above the HCl + acetylene asymptote. Using FTIR, Lee and co- workers reported a bimodal HCl rotational distribution and vibrational excitation extending up to v = 6. They assigned the low rotational component to the 4C channel based on simulations using the TS displacement vectors, but subsequent direct dynamics studies[129, 130] have shown that the low-J component is associated with the 3C channel, and the high-J component with the 4C pathway. Although the 3C channel results in vinylidene formation, to account for the fact that, at 193 nm, the 3C translational energy release is significantly larger than the magnitude of the barrier, Gordon and co- workers suggested[123-125] that some of the energy released in the isomerization to acetylene may be available for product recoil. This view was echoed in several subsequent studies and observed in some of the direct dynamics trajectories. This underscores the problem that precludes 193 nm dissociation as a route to synthesis of cold vinylidene: the excess energy yields vinylidene with such high internal excitation that the product vinylidene character will be diluted into many excited acetylene levels and lost. Thus, we turned to infrared photodissociation as a possible route to cold vinylidene.

IRMPD attracted a great deal of attention in the 1970s and 1980s, as it was found that molecules could be “heated” under collisionless conditions and the ground electronic state decomposition pathways could be studied in detail.[20, 21, 80, 131, 132] These studies generally employed universal mass spectrometric detection but lacked quantum state specific probes. In the intervening decades, state-resolved velocity map[49, 50] and DC slice imaging[54] have emerged as powerful tools in the study of photodissociation dynamics. However, the opportunities afforded by the combination of state-specific imaging with ground state IRMPD

have only recently been recognized, with the first such reports now appearing from our laboratory.[74, 133] Vinyl chloride represents an excellent system to exploit the virtues of this combination. In these experiments we dissociate vinyl chloride in a molecular beam using a TEA-CO_2 laser, then probe the HCl product state specifically using 2 + 1 resonant ionization. We obtained the rotational distribution for the HCl product in v = 0, and recorded images on a number of rotational levels in v = 0 and v = 1. In addition, we have performed direct dynamics trajectory studies to determine the translational energy release and product state distributions following excitation at energies just above the 3C-TS, both for comparison to experiment, and to probe the nascent C_2H_2 rotational excitation.

The well-studied 193 nm dissociation includes both 3C and 4C channels, in a ratio estimated from the rotational distributions in HCl to be 4:1. The rotational distribution for the 3C channel was seen in the earlier dynamics study[129] to reach a maximum around J = 5 and extend to J = 40. The 4C channel, on the other hand, extends broadly from J = 18 to 40 with undetectable population in low rotational levels. This high rotational excitation arises in part to the large translational energy release for the 4C channel.

6.2 Experimental

Vinyl chloride (Fluka) was diluted to 5% in He and expanded at 1000 Torr from a pulsed solenoid valve (Parker-General). The pulsed nozzle is fitted with a 0.5 mm bore diameter copper tube that was heated to 650 K. The expansion-cooled vinyl chloride beam was then intersected by two counter-propagating laser beams. The IR beam, at 10.6 μm, was produced by a grating-tuned TEA-CO_2 laser (GAM laser). The product HCl wasdetectedby 2+1 REMPI on two bands. The $E\,^1\Sigma^+ \leftarrow\leftarrow X\,^1\Sigma^+$ (0,0) band system, around 238 nm, was used for ion- imaging on selected rotational levels, although it generates HCl^+, Cl^+, or H^+, depending on the probed rotational

level. The 238 nm radiation was generated by mixing the third harmonic of an injection-seeded Nd:YAG laser with the fundamental output of a pulsed dye laser (Sirah, LDS 722 in ethanol) pumped by the second harmonic of the same Nd:YAG laser. For the $F\,^1\Delta_2 \leftarrow\leftarrow X\,^1\Sigma^+(0,0)$ and $f\,^3\Delta_2 \leftarrow\leftarrow X\,^1\Sigma^+$ (1,1) band systems,[134, 135] the wavelength was 242 nm, generated using the dye LDS 751 in DMSO. These transitions exclusively produce HCl^+, and were thus used to obtain the rotational distributions.[136] Populations were determined from REMPI spectra using appropriate two-photon line strength factors[137] after correcting for predissociation as described elsewhere.[138] The power of the 10.6 μm laser was ~90 mJ/pulse and focused by an f = 25 cm lens. The UV beam power was ~2.5 mJ/pulse. The resulting ions were accelerated through a time-of-flight tube toward a 120 mm microchannel plate detector coupled to a P-47 phosphor screen. DC sliced images[49, 50, 54] were captured using a USB CCD camera, and data acquisition was done using our own NuACQ program. Total translational energy distributions were obtained using the images captured.

6.3 Computational

The direct dynamics simulations were carried out using Gaussian 09 package[139] with the M06-2X density functional[140] and aug-cc-pVDZ basis set.[141] This functional was found to give satisfactory energetics compared to higher level CCSD(T)-F12/aug-cc-pVDZ calculations. The trajectories were initiated at the 3C saddle point and standard micro- canonical normal mode sampling was employed.[142] An addi- tional 7.0 kcal/mol energy was added to the imaginary- frequency mode. This energy was chosen as a compromise between the experimental energy (which is somewhat above the threshold for dissociation) and consideration of the computational cost of running direct-dynamics. Any spurious angular momentum was

removed, so the initial angular momentum was zero (J = 0) for all the trajectories. The step size is 5 au (0.121 fs), and the maximum number of steps for a trajectory is 4000 (483.8 fs). Each trajectory required roughly 24 h on a single node of our compute cluster. In total, 452 trajectories dissociated, and the total translational energy and angular momenta of the fragments were calculated and analyzed here.

6.4 Results and Discussion

Figure 6.1A shows the HCl v = 0 REMPI spectrum we obtain following IRMPD of vinyl chloride. No signal was detected in rotational levels 20 or 25, despite the fact that these levels are expected to be well-populated via the 4C pathway. The HCl rotational level populations obtained from the trajectory calculations are shown in Figure 6.1B. A Boltzmann fit (inset) gives a rotational temperature of 270 K for the experimental spectrum and 510 K for the trajectory results. This difference may be due in part to the additional 7 kcal/mol above the 3C- TS provided in the trajectory calculations.

DC slice images of a range of rotational levels of HCl in v = 0 and v = 1 are given in Figure 6.2, as well as the total translational energy distributions derived from the images. All of the images are isotropic and show low translational energy release, peaking at 3−5 kcal/mol with an average total translational energy of 4−5 kcal/mol. Results for HCl v = 1 are similar, although the signal is significantly weaker and the average translational energy release lower at 3 kcal/mol. The low translational energy release seen here is in stark contrast to the results at 193 nm, which peak at 15 kcal/mol and extend beyond 60 kcal/ mol. The translational energy distribution obtained from the trajectory data is also given in Figure 6.3, showing an average translational energy release of 2.5 kcal/mol, in good agreement with the experimental results. The low translational energy release, resembling the reverse barrier for the 3C-TS, combined

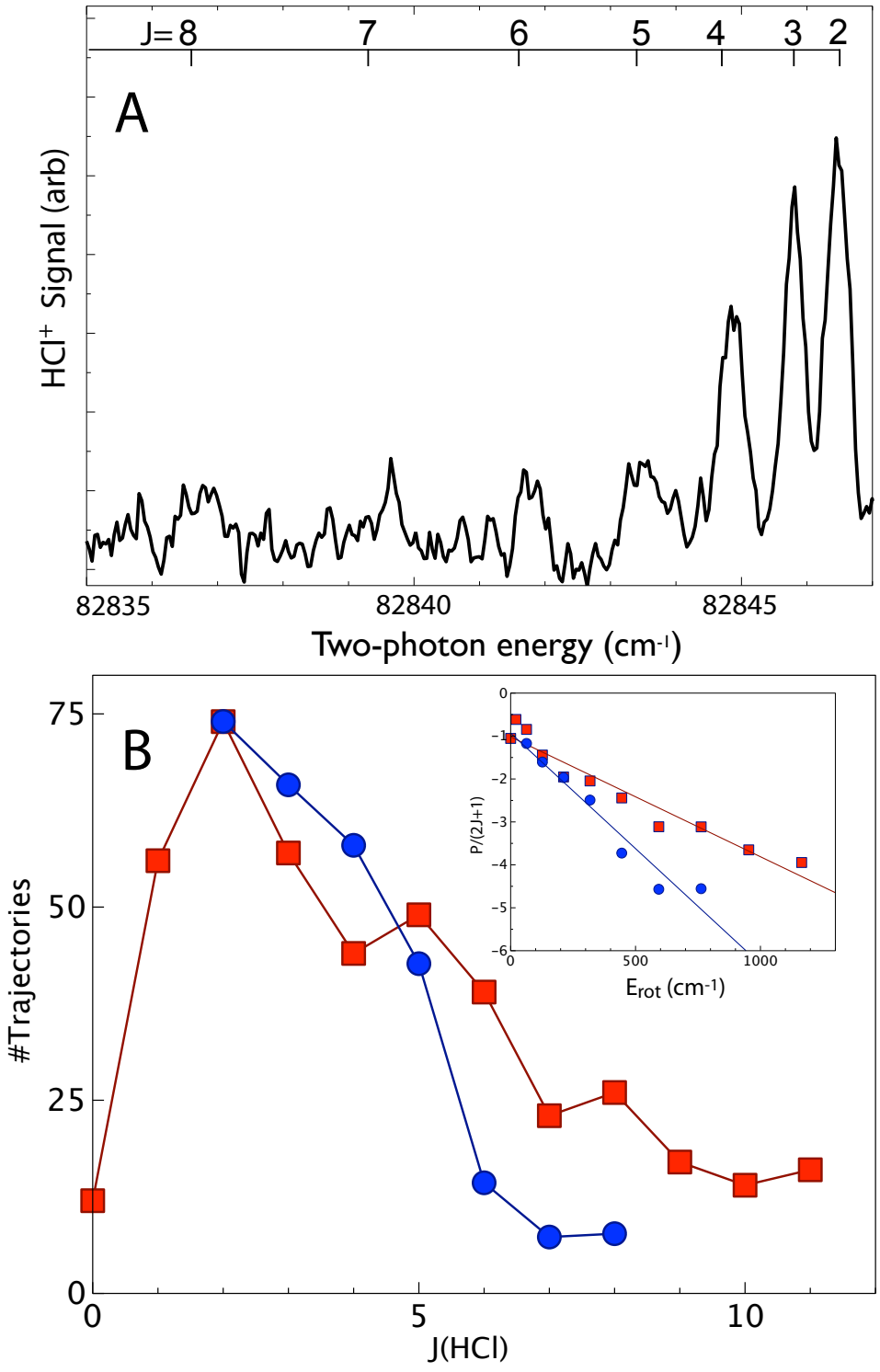

Figure 6.2: HCl (v = 0) rotational distributions following IRMPD of vinyl chloride. (A) Experimental REMPI spectrum; (B) trajectory results (red squares) and experimental populations (blue circles) with Boltzmann plot inset.

with low rotational excitation in HCl, indicate clearly that the product we detect originates in the 3C elimination of HCl from vinyl chloride, making vinylidene as a 1:1 coproduct. The good agreement with the theory for dissociation starting from the 3C-TS confirms this. The absence of the 4C product in our experiments is readily understood from the 3 kcal/mol higher energy of the 4C-TS, as well as entropic factors that favor the 3C channel. Although the trajectory calculations are performed for parent J = 0, and the infrared excitation populates a range of parent rotational levels, the IRMPD has a bias toward low J because it is sampling the high energy tail of the distribution in the right mode, which is a bias against excitation in the wrong mode (rotation). The fact that the experimental HCl rotational distribution is cold and consistent with the theory confirms that parent rotation does not have a large impact on the product distributions. We note also that a global potential energy surface will be developed for vinyl chloride in the near future, and could be used in quantum calculations of this dissociation.

We now consider the predicted internal excitation in the vinylidene coproduct. For this we turn exclusively to the trajectory calculations, as information about vinylidene is not yet directly available from experiment. The results, obtained from a classical calculation of the C_2H_2 rotational excitation in 10 or lower. This low rotational excitation in the C_2H_2 product is extremely significant. Previous attempts to probe vinylidene directly employed photodissociation of vinyl cyanide at 193 nm, which generates HCN/HNC and acetylene/vinylidene fragments at energies far above the HCN + vinylidene threshold.[113, 143] Millimeter wave spectra revealed the nascent vibrational population distributions in both HCN and HNC.[39] However, no millimeter wave transitions from the expected vinylidene and local-bender vibrationally excited acetylene coproducts were detected, despite their expected comparable populations and comparable electric dipole transition moments. The reason for the absence of vinylidene from the

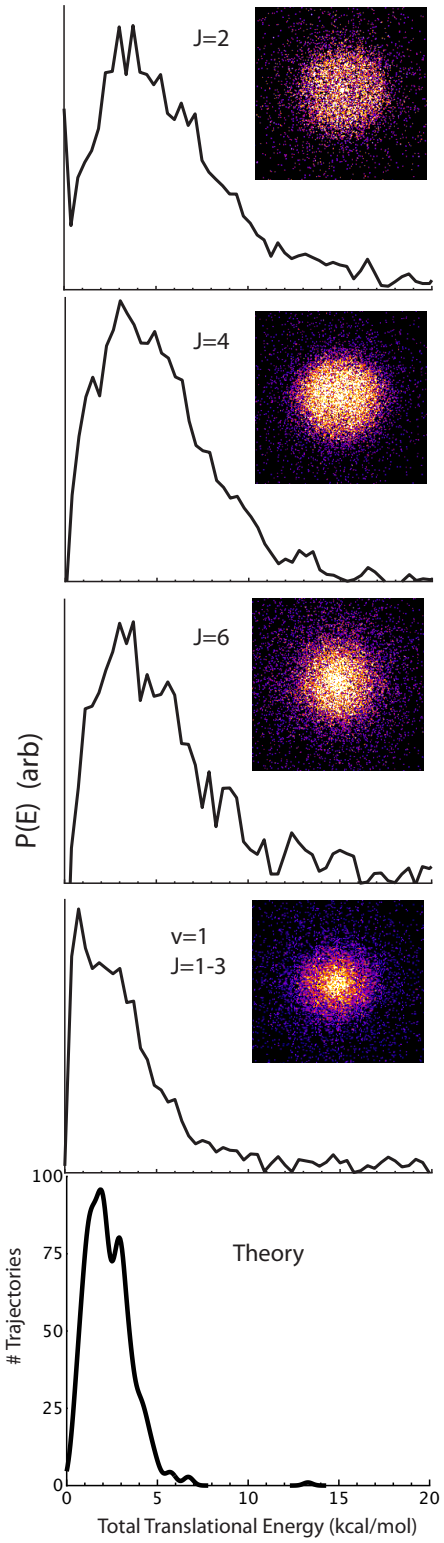

Figure 6.3: HCl DC sliced images and total translational energy distributions for indicated rotational level, and corresponding trajectory results.

millimeter wave spectrum is that 193 nm photolysis of VCN produces vinylidene at very high rotational excitation. Perry and Herman showed that high rotation results in complete intramolecular vibrational relaxation (IVR) on the acetylene side of the isomerization barrier.[121, 122] As a result, vinylidene (and local- bender acetylene) character is diluted into many eigenstates, thereby reducing both the single rotation-vibration level populations and the transition moments, rendering all J = 0− 1 transitions undetectably weak. In the absence of C_2H_2 rotational excitation, eigenstates of predominantly vinylidene character are seen to persist.

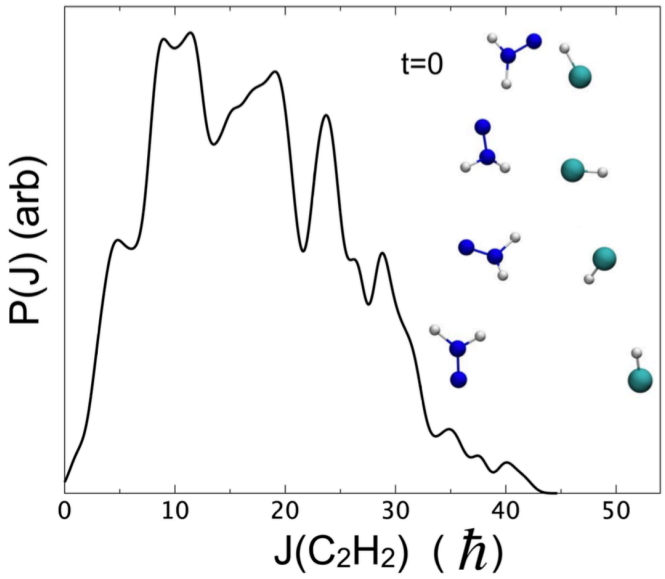

Figure 6.4: C_2H_2 total rotational distribution obtained from trajectories. Inset shows a typical trajectory that persists as vinylidene, with snapshots every 90 fs.

Also shown in Figure 6.4 is a typical trajectory that persists as vinylidene, to highlight that the 3C elimination indeed initially forms the vinylidene structure. However, one must refrain from thinking too classically about this. In these experiments, a chemical "pluck" of the system creates, at t = 0, a pure vinylidene quantum mechanical superposition state. The time evolution of this initially formed state will depend on the number, nature, and energy spacings of the eigenstates that express this t = 0 state. Different vinylidene vibrational levels will have different

time behaviors. In general, there will be a fast initial decay of the phased-up vinylidene character. However, if there are only two or three dominant eigenstates, the vinylidene character will be manifest as nearly perfectly recurring quantum beats, as seen in the CEI experiments. The present experiments show clearly that the chemical pluck (IRMPD of vinyl chloride) creates t = 0 vinylidene states (via the 3C transition state). That is, IRMPD of vinyl chloride gives rise to 3C elimination of HCl with the coproduct C_2H_2 born as vinylidene with low rotational excitation. This v = 0 vinylidene state will have a particularly simple quantum mechanical eigenstate description, ideal conditions for future direct spectroscopic detection.

CHAPTER 7 CONCLUSION AND PROSPECTUS

This dissertation summarizes the results obtained using DC slice imaging as a probe of ground state photodissociation phenomena of various systems. An interesting and fundamentally important phenomenon discovered in the Suits group is the "roaming radical" pathway in photodissociation. Although first observed experimentally nearly a decade ago, a number of open questions remain as to what makes a molecule "roam", and what exact implications this pathway poses to traditional transition state theory. In this work, DC slice imaging coupled with IRMPD provides unique insight into the roaming picture that is not afforded by the UV pump/probe experiments often used to study molecular photodissociation. IRMPD serves as a direct probe of those products dissociating exclusively on the ground electronic state, which is where the majority of roaming reactions take place.

In an effort to more deeply understand the complexities of roaming, both visible photodissociation and IRMPD was employed to study NO_3, which exhibits roaming on both the ground and excited electronic states. The results obtained in this work show no distinct difference in the product energy distributions between the UV and IRMPD experiments, suggesting a different relaxation pathway for the dissociation of the excited NO_3 molecule. Indeed, it was not possible in earlier UV experiments to disentangle the dynamics associated with these two states; however, it was possible to do so through the combination of IRMPD and DC-slice ion imaging.

While IRMPD offers the unique ability to probe products dissociating along the ground electronic state exclusively, the DC-slice imaging detection method alone offers deep insight into the underlying dynamics of molecular photodissociation. It is possible to extract key features including product energy distributions, branching ratios, and population distributions state-

specifically with the high-resolution inherent to the DC-slice imaging approach used here. Application to the photodissociation of nitromethane and methyl nitrite allowed for the unambiguous observation of the isomerization between these two systems before dissociating into products. Interestingly, the low translational energy release of the photofragments of methyl nitrite closely resembles the translational energy release observed in the roaming dissociation of nitromethane, suggesting that the isomerization itself is roaming-mediated. In order to generalize this concept of roaming-mediated isomerization (RMI) in nitro- compounds, studies were extended for the C-2, C-3, and C-4 systems. Here, it was found that RMI predominates in the nitroethane and nitropropane dissociation, despite the fact that the concerted molecular elimination (CME) channel is significantly lower in energy. An exception to these systems is nitrobutane, which shows distinct dynamics due to the 6-membered transition state, or perhaps an alternative dissociation pathway. A complete understanding of this species requires additional computational work, while the strength of the DC-slice imaging approach is highlighted in its ability to unravel the unique underlying dynamics of these closely related systems.

In addition to offering exclusive formation of ground state dissociation products, IRMPD was used in this work as a means to produce the highly unstable and long sought after radical species: vinylidne. In these experiments, IRMPD was performed on the precursor vinyl chloride in order to produce cold vinylidene. REMPI spectra and DC-sliced images of the HCl product revealed the formation of vibrationally and rotationally cold vinylidene. On the basis of the translational energy distributions in conjunction with the calculated rotational temperature and trajectory calculations, it was shown that indeed, photodissociation of vinyl chloride yields HCl and vinylidene products. These findings suggest an ideal way in which to produce vibrationally and rotationally cold vinylidene through IRMPD, and open the door for future high-resolution

spectroscopic experiments on this important molecule that has not yet been isolated in the gas phase.

This thesis highlights the combination of two powerful techniques from two very different eras: DC-sliced ion imaging, a fairly recent advance in experimental chemical physics; and IRMPD, a technique heavily utilized in the 1970's and 1980's, but largely abandoned upon the introduction of steady-state, high power, and high-resolution lasers. This work demonstrates that the combined approach offers the ability to produce rotationally and vibrationally cold transient species through state-specific photodissociation experiments; to characterize important phenomena such as isomerization by way of roaming; and finally, to gain insight into the ubiquitous roaming phenomenon in a unique way by exclusively examining ground state dissociation where the majority of roaming takes place. These experiments merely scratch the surface of what can be done in the laboratory to unravel complex dissociation dynamics through the use of DC-slice imaging coupled with IRMPD, but should serve as motivation for future investigations which can greatly benefit from exploiting the combination of these two complimentary and powerful techniques.

BIBLIOGRAPHY

1. Isenor, N.R. and M.C. Richardson, *DISSOCIATION AND BREAKDOWN OF MOLECULAR GASES BY PULSED CO2 LASER RADIATION.* Applied Physics Letters, 1971. **18**(6): p. 224-226.
2. Isenor, N.R. and M.C. Richardson, *Spatial structure of the luminescence induced in SiF4 gas by 10.6 μ radiation.* Optics Communications, 1971. **3**(5): p. 360-362.
3. Isenor, N.R., et al., *CO2 Laser-Induced Dissociation of SiF4 Molecules into Electronically Excited Fragments.* Canadian Journal of Physics, 1973. **51**(12): p. 1281-1287.
4. M.J. Coggiola, P.A.S.Y.T.L.a.Y.R.S., Phys. Roy. Letters 1977. **38**: p. 17.
5. Aa.S. Sudbø, P.A.S., E.R. Grant, V.R. Shen, V.T. Lee, J. Chem. Phys., 1978. **68,** : p. 1306
6. Sudbø, A.S., et al., *Molecular-beam studies of laser-induced multiphoton dissociation*. 1986: Springer.
7. Ambartzumian, R.V. and V.S. Letokhov, *Selective dissociation of polyatomic molecules by intense infrared laser fields.* Accounts of Chemical Research, 1977. **10**(2): p. 61-67.
8. Ambartzumian, R.V., et al., *The visible luminescence kinetics of BCl3 in the field of a high-power CO2 Laser.* Chemical Physics Letters, 1974. **25**(4): p. 515-518.
9. Maier, J.P., et al., *Ultrashort vibrational population lifetime of large polyatomic molecules in the vapor phase.* Chemical Physics Letters, 1977. **46**(3): p. 527-530.
10. Bomse, D.S. and J.L. Beauchamp, *Selective enhancement of bimolecular reaction rates by over three orders of magnitude using low intensity CW infrared laser radiation.* Journal of the American Chemical Society, 1980. **102**(11): p. 3967-3969.

11. Bomse, D.S., D.W. Berman, and J.L. Beauchamp, *Energetics of the rearrangement of neutral and ionized perfluorocyclopropane to perfluoropropylene. Use of infrared multiphoton dissociation spectra to identify structural isomers of molecular ions.* Journal of the American Chemical Society, 1981. **103**(14): p. 3967-3971.

12. Grant, E.R., et al., *The extent of energy randomization in the infrared multiphoton dissociation of SF6.* Chemical Physics Letters, 1977. **52**(3): p. 595-599.

13. Schulz, P.A., et al., *Multiphoton dissociation of SF6 by a molecular beam method.* The Journal of Chemical Physics, 1980. **72**(9): p. 4985-4995.

14. Berrie, C.L., et al., *Infrared Multiphoton Dissociation of Acetone in a Molecular Beam.* The Journal of Physical Chemistry A, 2001. **105**(12): p. 2557-2562.

15. Longfellow, C.A. and Y.T. Lee, *Methane Loss in the Infrared Multiphoton Dissociation of Acetic Acid.* The Journal of Physical Chemistry, 1995. **99**(42): p. 15532-15537.

16. Krajnovich, D., et al., *Competition between atomic and molecular chlorine elimination in the infrared multiphoton dissociation of CF2Cl2.* The Journal of Chemical Physics, 1982. **77**(12): p. 5977-5989.

17. Sudbo/, A.S., et al., *Three and four center elimination of HCl in the multiphoton dissociation of halogenated hydrocarbons.* The Journal of Chemical Physics, 1978. **69**(6): p. 2312-2322.

18. Zhao, X., E.J. Hintsa, and Y.T. Lee, *Infrared multiphoton dissociation of RDX in a molecular beam.* The Journal of Chemical Physics, 1988. **88**(2): p. 801-810.

19. Wodtke, A.M., E.J. Hintsa, and Y.T. Lee, *The observation of CH3O in the collision free multiphoton dissociation of CH3NO2.* The Journal of Chemical Physics, 1986. **84**(2): p. 1044-1045.

20. Wodtke, A.M., E.J. Hintsa, and Y.T. Lee, *Infrared multiphoton dissociation of three nitroalkanes.* The Journal of Physical Chemistry, 1986. **90**(16): p. 3549-3558.

21. Hintsa, E.J., A.M. Wodtke, and Y.T. Lee, *Infrared multiphoton dissociation of ethyl and methyl acetate.* The Journal of Physical Chemistry, 1988. **92**(19): p. 5379-5387.

22. Robinson, P.J.H., K. A., *Unimolecular reactions*. 1972: Willey, London.

23. Grant, E.R., et al., *Is Multiphoton Dissociation of Molecules a Statistical Thermal Process?* Physical Review Letters, 1978. **40**(2): p. 115-118.

24. Schulz, P.A., *MULTIPHOTON DISSOCIATION OF POLY ATOMIC MOLECULES*. 2010.

25. A. S. Sudbø, P.A.S., Y. R. Shen, and Y. T. Lee,, *Multiple-Photon Excitation and Dissociation of Polyatomic Molecules*, ed. C. Cantrell. Vol. 35. 1986: Springer,Berlin.

26. Bowman, J.M. and B.C. Shepler, *Roaming Radicals.* Annual Review of Physical Chemistry, 2011. **62**(1): p. 531-553.

27. Herath, N. and A.G. Suits, *Roaming Radical Reactions.* The Journal of Physical Chemistry Letters, 2011. **2**(6): p. 642-647.

28. Townsend, D., et al., *The Roaming Atom: Straying from the Reaction Path in Formaldehyde Decomposition.* Science, 2004. **306**(5699): p. 1158-1161.

29. Lahankar, S.A., et al., *The roaming atom pathway in formaldehyde decomposition.* The Journal of Chemical Physics, 2006. **125**(4): p. 044303.

30. Suits, A.G., S.D. Chambreau, and S.A. Lahankar, *State-correlated DC slice imaging of formaldehyde photodissociation: roaming atoms and multichannel branching.* International Reviews in Physical Chemistry, 2007. **26**(4): p. 585-607.

31. Goncharov, V., N. Herath, and A.G. Suits, *Roaming Dynamics in Acetone Dissociation.* The Journal of Physical Chemistry A, 2008. **112**(39): p. 9423-9428.

32. Houston, P.L. and S.H. Kable, *Photodissociation of acetaldehyde as a second example of the roaming mechanism.* Proceedings of the National Academy of Sciences, 2006. **103**(44): p. 16079-16082.

33. Sivaramakrishnan, R., J.V. Michael, and S.J. Klippenstein, *Direct Observation of Roaming Radicals in the Thermal Decomposition of Acetaldehyde.* The Journal of Physical Chemistry A, 2010. **114**(2): p. 755-764.

34. Harding, L.B., Y. Georgievskii, and S.J. Klippenstein, *Roaming Radical Kinetics in the Decomposition of Acetaldehyde.* The Journal of Physical Chemistry A, 2010. **114**(2): p. 765-777.

35. Grubb, M.P., et al., *No Straight Path: Roaming in Both Ground- and Excited-State Photolytic Channels of NO3 → NO + O2.* Science, 2012. **335**(6072): p. 1075-1078.

36. Grubb, M.P., et al., *Evidence of Roaming Dynamics and Multiple Channels for Molecular Elimination in NO3 Photolysis.* The Journal of Physical Chemistry Letters, 2010. **1**(16): p. 2455-2458.

37. Grubb, M.P., et al., *Ion imaging study of NO3 radical photodissociation dynamics: characterization of multiple reaction pathways.* The Journal of Physical Chemistry A, 2011. **115**(15): p. 3218-3226.

38. Xiao, H., S. Maeda, and K. Morokuma, *Excited-State Roaming Dynamics in Photolysis of a Nitrate Radical.* The Journal of Physical Chemistry Letters, 2011. **2**(9): p. 934-938.

39. Prozument, K., et al., *A Signature of Roaming Dynamics in the Thermal Decomposition of Ethyl Nitrite: Chirped-Pulse Rotational Spectroscopy and Kinetic Modeling.* The Journal of Physical Chemistry Letters, 2014. **5**(21): p. 3641-3648.

40. Chen, C., et al., *Quasiclassical trajectory calculations of the HO 2+ NO reaction on a global potential energy surface.* Physical Chemistry Chemical Physics, 2009. **11**(23): p. 4722-4727.

41. Kamarchik, E., et al., *Roaming pathway leading to unexpected water+ vinyl products in C2H4OH dissociation.* The Journal of Physical Chemistry Letters, 2010. **1**(20): p. 3058-3065.

42. Sivaramakrishnan, R., et al., *Roaming radicals in the thermal decomposition of dimethyl ether: Experiment and theory.* Combustion and Flame, 2011. **158**(4): p. 618-632.

43. Thomas, J.O., K.E. Lower, and C. Murray, *Observation of NH X3Σ–as a primary product of methylamine photodissociation: evidence of roaming-mediated intersystem crossing?* The journal of physical chemistry letters, 2012. **3**(10): p. 1341-1345.

44. Rodriguez, J.D., et al., *A velocity map imaging study of the photodissociation of the A state of ammonia.* Physical Chemistry Chemical Physics, 2014. **16**(2): p. 406-413.

45. Hause, M.L., et al., *Roaming-mediated isomerization in the photodissociation of nitrobenzene.* Nat Chem, 2011. **3**(12): p. 932-937.

46. Homayoon, Z., et al., *Experimental and Theoretical Studies of Roaming Dynamics in the Unimolecular Dissociation of CH3NO2 to CH3O + NO*, in *Zeitschrift für Physikalische Chemie*. 2013. p. 1267.

47. Homayoon, Z. and J.M. Bowman, *Quasiclassical Trajectory Study of CH3NO2 Decomposition via Roaming Mediated Isomerization Using a Global Potential Energy Surface.* The Journal of Physical Chemistry A, 2013. **117**(46): p. 11665-11672.

48. Zhu, R.S. and M.C. Lin, *CH3NO2 decomposition/isomerization mechanism and product branching ratios: An ab initio chemical kinetic study.* Chemical Physics Letters, 2009. **478**(1–3): p. 11-16.

49. Eppink, A.T. and D.H. Parker, *Velocity map imaging of ions and electrons using electrostatic lenses: Application in photoelectron and photofragment ion imaging of molecular oxygen.* Review of Scientific Instruments, 1997. **68**(9): p. 3477-3484.

50. Chandler, D.W. and P.L. Houston, *Two‐dimensional imaging of state‐selected photodissociation products detected by multiphoton ionization.* The Journal of chemical physics, 1987. **87**(2): p. 1445-1447.

51. Gebhardt, C.R., et al., *Slice imaging: A new approach to ion imaging and velocity mapping.* Review of Scientific Instruments, 2001. **72**(10): p. 3848-3853.

52. Kitsopoulosa, T.N., C.R. Gebhardt, and T.P. Rakitzis, *Photodissociation study of CS2 at 193 nm using slice imaging.* imaging, 2001. **16**: p. 17.

53. Rakitzis, T.P. and T.N. Kitsopoulos, *Measurement of Cl and Br photofragment alignment using slice imaging.* Journal of Chemical Physics, 2002. **116**(21): p. 9228-9231.

54. Townsend, D., M.P. Minitti, and A.G. Suits, *Direct current slice imaging.* Review of scientific instruments, 2003. **74**(4): p. 2530-2539.

55. Grant, E.R., et al., *Multiphoton Dissociation of Polyatomic Molecules Studied with a Molecular Beam*, in *Laser Spectroscopy III: Proceedings of the Third International*

Conference, Jackson Lake Lodge, Wyoming, USA, July 4–8, 1977, J.L. Hall and J.L. Carlsten, Editors. 1977, Springer Berlin Heidelberg: Berlin, Heidelberg. p. 94-101.

56. Butler, L., et al., *The Photodissociation of Nitromethane at 193 nm.* The Journal of chemical physics, 1983. **79**(4): p. 1708-1722.

57. Moss, D., K. Trentelman, and P. Houston, *193 nm photodissociation dynamics of nitromethane.* The Journal of chemical physics, 1992. **96**(1): p. 237-247.

58. Guo, Y., A. Bhattacharya, and E. Bernstein, *Photodissociation dynamics of nitromethane at 226 and 271 nm at both nanosecond and femtosecond time scales.* The Journal of Physical Chemistry A, 2008. **113**(1): p. 85-96.

59. McKee, M.L., *Ab initio study of rearrangements on the nitromethane potential energy surface.* Journal of the American Chemical Society, 1986. **108**(19): p. 5784-5792.

60. Nguyen, M.T., et al., *Nitromethane-methyl nitrite rearrangement: A persistent discrepancy between theory and experiment.* The Journal of Physical Chemistry A, 2003. **107**(21): p. 4286-4291.

61. Hu, W.-F., et al., *Theoretical study of the CH3NO2 unimolecular decomposition potential energy surface.* The Journal of Physical Chemistry A, 2002. **106**(32): p. 7294-7303.

62. McKee, M.L., *MCSCF study of the rearrangement of nitromethane to methyl nitrite.* The Journal of Physical Chemistry, 1989. **93**(21): p. 7365-7369.

63. Saxon, R.P. and M. Yoshimine, *Theoretical study of nitro-nitrite rearrangement of CH3NO2.* Canadian Journal of Chemistry, 1992. **70**(2): p. 572-579.

64. Hansen, N., et al., *Ion dissociation dynamics of the chlorine azide cation (ClN3+) investigated by velocity map imaging.* Journal of Chemical Physics, 2003. **118**(23): p. 10485-10493.

65. Cruse, H. and T. Softley, *Velocity-map imaging study of the photodissociation of acetaldehyde.* The Journal of chemical physics, 2005. **122**(12): p. 124303-124303.

66. Zhu, R., P. Raghunath, and M. Lin, *Effect of Roaming Transition States upon Product Branching in the Thermal Decomposition of CH3NO2.* The Journal of Physical Chemistry A, 2013. **117**(32): p. 7308-7313.

67. Mulliken, R.S. and A. Christy, *Λ-type doubling and electron configurations in diatomic molecules.* Physical Review, 1931. **38**(1): p. 87.

68. Alexander, M., et al., *A nomenclature for Λ-doublet levels in rotating linear molecules.* The Journal of chemical physics, 1988. **89**(4): p. 1749-1753.

69. Andresen, P. and E.W. Rothe, *Analysis of chemical dynamics via Λ doubling: Directed lobes in product molecules and transition states.* The Journal of chemical physics, 1985. **82**(8): p. 3634-3640.

70. King, D.S. and J.C. Stephenson, *Infrared multiphoton dissociation of methyl nitrite in a molecular beam: Internal states of the nitric oxide fragment.* The Journal of chemical physics, 1985. **82**(5): p. 2236-2239.

71. Atkins, C. and G. Hancock, *The 355 nm Nitrite.* Laser Chem, 1988. **9**: p. 195-208.

72. Lahmani, F., C. Lardeux, and D. Solgadi, *Rotational and electronic anisotropy in no X 2 Π from the photodissociation of CH 3 ONO.* Chemical physics letters, 1986. **129**(1): p. 24-30.

73. Brühlmann, U., M. Dubs, and J.R. Huber, *Photodissociation of methylnitrite: State distributions, recoil velocity distribution, and alignment effects of the NO (X 2Π) photofragment.* The Journal of chemical physics, 1987. **86**(3): p. 1249-1257.

74. Dey, A., et al., *Photodissociation dynamics of nitromethane and methyl nitrite by infrared multiphoton dissociation imaging with quasiclassical trajectory calculations: Signatures of the roaming pathway.* The Journal of Chemical Physics, 2014. **140**(5): p. 054305.

75. Isegawa, M., et al., *Ab initio reaction pathways for photodissociation and isomerization of nitromethane on four singlet potential energy surfaces with three roaming paths.* The Journal of chemical physics, 2014. **140**(24): p. 244310.

76. Annesley, C.J., et al., *Thermal Dissociation and Roaming Isomerization of Nitromethane: Experiment and Theory.* The Journal of Physical Chemistry A, 2015. **119**(28): p. 7872-7893.

77. Sudbo, A.S., et al., *Simple bond rupture reactions in multiphoton dissociation of molecules.* The Journal of Chemical Physics, 1979. **70**(2): p. 912-929.

78. Krajnovich, D., et al., *Competition between atomic and molecular chlorine elimination in the infrared multiphoton dissociation of CF2Cl2.* The Journal of Chemical Physics, 1982. **77**(12): p. 5977-5989.

79. Schulz, P., et al., *Multiphoton dissociation of SF6 by a molecular beam method.* The Journal of Chemical Physics, 1980. **72**(9): p. 4985-4995.

80. Hancock, G. and K.G. McKendrick, *Intramolecular rearrangement in the infrared multiple-photon dissociation of dichlorodifluoroethylene.* The Journal of Physical Chemistry, 1988. **92**(7): p. 1839-1846.

81. Grant, E., et al., *The extent of energy randomization in the infrared multiphoton dissociation of SF6.* Chemical Physics Letters, 1977. **52**(3): p. 595-599.

82. Sudbo, A.S., et al., *Three and four center elimination of HCl in the multiphoton dissociation of halogenated hydrocarbons.* The Journal of Chemical Physics, 1978. **69**(6): p. 2312-2322.

83. Huisken, F., et al., *Competing dissociation channels in the infrared multiphoton decomposition of ethyl vinyl ether.* The Journal of Chemical Physics, 1983. **78**(6): p. 3806-3815.

84. Li, W., et al., *Megapixel ion imaging with standard video.* Review of Scientific Instruments, 2005. **76**(6): p. 063106.

85. Luque, J. and D. Crosley, *LIFBASE: Database and Spectral Simulation Program (Version 1.5), 1999, SRI Int.* Rep. MP: p. 99-009.

86. Denis, P.A., et al., *Density functional study of the decomposition pathways of nitroethane and 2-nitropropane.* Physical Chemistry Chemical Physics, 2003. **5**(9): p. 1730-1738.

87. Wang, Q., D. Ng, and M.S. Mannan, *Study on the reaction mechanism and kinetics of the thermal decomposition of nitroethane.* Industrial & Engineering Chemistry Research, 2009. **48**(18): p. 8745-8751.

88. Asatryan, R., J.W. Bozzelli, and J.M. Simmie, *Thermochemistry of methyl and ethyl nitro, RNO2, and nitrite, RONO, organic compounds.* The Journal of Physical Chemistry A, 2008. **112**(14): p. 3172-3185.

89. Nikolaeva, E.V., et al., *The role of nitro-nitrite rearrangement in the mechanism of monomolecular decomposition of aliphatic nitro compounds.* Butlerov Commun, 2001. **3**: p. 15-23.

90. Lahankar, S.A., et al., *Energy dependence of the roaming atom pathway in formaldehyde decomposition.* The Journal of Chemical Physics, 2007. **126**(4): p. 044314.

91. Cramarossa, F. and H. Johnston, *Infrared Absorption by Symmetrical NO3 Free Radical in the Gas Phase.* The Journal of Chemical Physics, 1965. **43**(2): p. 727-731.

92. Magnotta, F. and H.S. Johnston, *Photodissociation quantum yields for the NO3 free radical.* Geophysical Research Letters, 1980. **7**(10): p. 769-772.

93. Eisfeld, W. and K. Morokuma, *Ab initio investigation of the vertical and adiabatic excitation spectrum of NO3.* Journal of Chemical Physics, 2001. **114**(21): p. 9430-9440.

94. Stanton, J.F., *On the vibronic level structure in the NO3 radical. I. The ground electronic state.* The Journal of chemical physics, 2007. **126**(13): p. 134309.

95. F. Stanton, J., *On the vibronic level structure in the NO3 radical: II. Adiabatic calculation of the infrared spectrum.* Molecular Physics, 2009. **107**(8-12): p. 1059-1075.

96. Hirota, E., et al., *Vibronic interactions in the NO3 radical.* The Journal of chemical physics, 1991. **95**(2): p. 771-775.

97. Davis, H.F., et al., *Dissociation energy and photochemistry of nitrogen trioxide.* The Journal of Physical Chemistry, 1993. **97**(10): p. 2172-2180.

98. Mikhaylichenko, K., et al., *Unimolecular decomposition of NO3: The NO+ O2 threshold regime.* The Journal of chemical physics, 1996. **105**(16): p. 6807-6817.

99. Johnston, H.S., H.F. Davis, and Y.T. Lee, *NO3 photolysis product channels: Quantum yields from observed energy thresholds.* The Journal of Physical Chemistry, 1996. **100**(12): p. 4713-4723.

100. Cantrell, C.A., et al., *Kinetic study of the nitrate free radical (NO3)-formaldehyde reaction and its possible role in nighttime tropospheric chemistry.* The Journal of Physical Chemistry, 1985. **89**(1): p. 139-146.

101. Suits, A.G., *Roaming atoms and radicals: a new mechanism in molecular dissociation.* Acc. Chem. Res, 2008. **41**(7): p. 873-881.

102. Bowman, J.M., *Roaming.* Molecular Physics, 2014. **112**(19): p. 2516-2528.

103. Grubb, M.P., M.L. Warter, and S.W. North, *Stereodynamics of multistate roaming.* Physical Chemistry Chemical Physics, 2012. **14**(19): p. 6733-6740.

104. Fu, B., et al., *Quasiclassical Trajectory Studies of the Photodissociation Dynamics of NO3 from the D0 and D1 Potential Energy Surfaces.* Journal of chemical theory and computation, 2013. **9**(2): p. 893-900.

105. Douglas, A., *Anomalously long radiative lifetimes of molecular excited states.* The Journal of Chemical Physics, 1966. **45**(3): p. 1007-1015.

106. Carter, R.T., et al., *A high-resolution study of the NO 3 radical produced in a supersonic jet.* Chemical physics letters, 1996. **257**(3): p. 297-302.

107. Xiao, H., S. Maeda, and K. Morokuma, *Global Ab Initio Potential Energy Surfaces for Low-Lying Doublet States of NO3.* Journal of Chemical Theory and Computation, 2012. **8**(8): p. 2600-2605.

108. Earls, L.T., *Intensities in Π 2− Σ 2 Transitions in Diatomic Molecules.* Physical Review, 1935. **48**(5): p. 423.

109. Nelson, H., L. Pasternack, and J. McDonald, *Excited state dynamics of NO3.* The Journal of chemical physics, 1983. **79**(9): p. 4279-4284.

110. Martínez, T.J., *Ab initio molecular dynamics around a conical intersection: Li (2p)+ H 2.* Chemical physics letters, 1997. **272**(3): p. 139-147.

111. Jacobson, M.P. and R.W. Field, *Acetylene at the Threshold of Isomerization.* The Journal of Physical Chemistry A, 2000. **104**(14): p. 3073-3086.

112. Chen, C., et al., *Evidence for vinylidene production in the photodissociation of the allyl radical.* The Journal of Physical Chemistry Letters, 2010. **1**(12): p. 1875-1880.

113. Homayoon, Z., et al., *Ab initio and RRKM study of the HCN/HNC elimination channels from vinyl cyanide.* The Journal of Physical Chemistry A, 2011. **115**(6): p. 979-985.

114. Burnett, S.M., et al., *Observation of X 1 A 1 vinylidene by photoelectron spectroscopy of the C 2 H 2− ion.* Chemical physics letters, 1983. **100**(2): p. 124-128.

115. Ervin, K.M., J. Ho, and W.C. Lineberger, *A study of the singlet and triplet states of vinylidene by photoelectron spectroscopy of H2C= C−, D2C= C−, and HDC= C−. Vinylidene–acetylene isomerization.* The Journal of chemical physics, 1989. **91**(10): p. 5974-5992.

116. Levin, J., et al., *Study of unimolecular reactions by Coulomb explosion imaging: the nondecaying vinylidene.* Physical review letters, 1998. **81**(16): p. 3347.

117. Zou, S. and J.M. Bowman, *Full dimensionality quantum calculations of acetylene/vinylidene isomerization.* The Journal of chemical physics, 2002. **117**(12): p. 5507-5510.

118. Xu, D., et al., *A scaled ab initio potential energy surface for acetylene and vinylidene.* Chemical physics letters, 2003. **377**(5): p. 582-588.

119. Han, H., A. Li, and H. Guo, *Toward spectroscopically accurate global ab initio potential energy surface for the acetylene-vinylidene isomerization.* The Journal of chemical physics, 2014. **141**(24): p. 244312.

120. Ren, Y. and W. Bian, *Mode-Specific Tunneling Splittings for a Sequential Double-Hydrogen Transfer Case: An Accurate Quantum Mechanical Scheme.* The journal of physical chemistry letters, 2015. **6**(10): p. 1824-1829.

121. Perry, D.S., et al., *Hierarchies of intramolecular vibration–rotation dynamical processes in acetylene up to 13,000 cm− 1.* Molecular physics, 2012. **110**(21-22): p. 2687-2705.

122. Perry, D.S., et al., *Vibration–rotation alchemy in acetylene (12C2H2), at low vibrational excitation: from high resolution spectroscopy to fast intramolecular dynamics.* Molecular physics, 2010. **108**(7-9): p. 1115-1132.

123. Huang, Y., et al., *Speed distributions of the photofragments of vinyl chloride determined by direct inversion of Doppler profiles.* Chemical physics letters, 1994. **229**(6): p. 621-627.

124. Huang, Y., et al., *The ultraviolet photodissociation dynamics of d1-vinyl chloride.* The Journal of chemical physics, 1993. **99**(4): p. 2752-2759.

125. Reilly, P.T., Y. Xie, and R.J. Gordon, *Product state distribution in the photodissociation of vinyl chloride at 193 nm.* Chemical physics letters, 1991. **178**(5): p. 511-516.

126. Lin, S.-R., et al., *Three-center versus four-center elimination in photolysis of vinyl fluoride and vinyl bromide at 193 nm: Bimodal rotational distribution of HF and HBr (v 5) detected with time-resolved Fourier transform spectroscopy.* The Journal of Chemical Physics, 2001. **114**(17): p. 7396-7406.

127. Blank, D.A., et al., *Primary and secondary processes in the 193 nm photodissociation of vinyl chloride.* The Journal of chemical physics, 1998. **108**(13): p. 5414-5425.

128. Riehl, J.F. and K. Morokuma, *An ab initio molecular orbital study of the unimolecular dissociation reactions of vinylchloride.* The Journal of chemical physics, 1994. **100**(12): p. 8976-8990.

129. Martınez-Núnez, E., et al., *Further investigation of the HCl elimination in the photodissociation of vinyl chloride at 193 nm: a direct MP2/6-31G (d, p) trajectory study.* Chemical physics letters, 2004. **386**(4): p. 225-232.

130. Núñez, E.M., et al., *A direct classical trajectory study of HCl elimination from the 193 nm photodissociation of vinyl chloride.* The Journal of Physical Chemistry A, 2003. **107**(38): p. 7611-7618.

131. Lussier, F.M. and J. Steinfeld, *Multiple infrared photon dissociation of vinyl chloride.* Chemical Physics Letters, 1977. **50**(2): p. 175-180.

132. P A Schulz, et al., *Multiphoton Dissociation of Polyatomic Molecules.* Annual Review of Physical Chemistry, 1979. **30**(1): p. 379-409.

133. Fernando, R., et al., *Visible/Infrared Dissociation of NO3: Roaming in the Dark or Roaming on the Ground?* The Journal of Physical Chemistry A, 2014. **119**(28): p. 7163-7168.

134. Green, D.S., G.A. Bickel, and S.C. Wallace, *(2 + 1) Resonance enhanced multiphoton ionization of hydrogen chloride in a pulsed supersonic jet: Vacuum wavenumbers of rotational lines with detailed band analysis for excited electronic states of H35Cl1.* Journal of Molecular Spectroscopy, 1991. **150**(2): p. 388-469.

135. Green, D.S. and S.C. Wallace, *Two‐photon spectroscopy, Rydberg~ valence interactions, and superexcited state dissociation of HCl probed by resonance enhanced multiphoton ionization.* The Journal of chemical physics, 1992. **96**(8): p. 5857-5877.

136. Rudić, S., et al., *The dynamics of formation of HCl products from the reaction of Cl atoms with methanol, ethanol, and dimethyl ether.* The Journal of Chemical Physics, 2002. **117**(12): p. 5692-5706.

137. Bray, R. and R.-M. Hochstrasser, *Two-photon absorption by rotating diatomic molecules.* Molecular Physics, 1976. **31**(4): p. 1199-1211.

138. Dagdigian, P.J., et al., *Detection of DCl by multiphoton ionization and determination of DCl and HCl internal state distributions.* The Journal of chemical physics, 1996. **105**(23): p. 10251-10262.

139. Frisch, M., et al., *Gaussian 09, Revision C. 01, Gaussian, Inc., Wallingford CT, 2009 Search PubMed;(b) Y. Zhao and DG Truhlar.* Theor. Chem. Acc, 2008. **120**: p. 215.

140. Zhao, Y. and D.G. Truhlar, *The M06 suite of density functionals for main group thermochemistry, thermochemical kinetics, noncovalent interactions, excited states, and transition elements: two new functionals and systematic testing of four M06-class functionals and 12 other functionals.* Theoretical Chemistry Accounts, 2008. **120**(1-3): p. 215-241.

141. Dunning Jr, T.H., *Gaussian basis sets for use in correlated molecular calculations. I. The atoms boron through neon and hydrogen.* The Journal of chemical physics, 1989. **90**(2): p. 1007-1023.

142. Hase, W.L., *Classical trajectory simulations: final conditions.* Encyclopedia of Computational Chemistry, 1998.

143. Wilhelm, M.J., et al., *Photodissociation of vinyl cyanide at 193 nm: Nascent product distributions of the molecular elimination channels.* The Journal of chemical physics, 2009. **130**(4): p. 044307.

ABSTRACT

STATE RESOLVED SLICED IMAGING OF INFRARED MULTIPHOTON DISSOCIATION

by

RAVIN LAKSHITHA FERNANDO

August 2016

Advisor : Dr. Arthur G. Suits

Major : Chemistry (Physical)

Degree : Doctor of Philosophy

This dissertation focuses on unimolecular dissociations of molecules under colissionless conditions with IRMPD. IRMPD was used as the dissociation technique in these studies since roaming type dissociations predominates from the ground electronic state. DC slice imaging was used with REMPI as the detection technique to study the products in a state selective manner to understand the nano scale dynamics of unimolecular dissociations. In the investigation of photodissociation dynamics of nitromethane and methyl nitrite with IRMPD, nitromethane show very low translational energy release of the photofragments and resemble the “roaming” pathway in the dissociation of nitromethane. The difference in the intensities of the averaged images show the presence of the lambda doublet propensity during the dissociation of nitromethane. In contrast, methyl nitrite does not show lambda doublet propensity while giving extra few kcal/mol during the dissociation into products relative to nitroethane supporting the conclusion of roaming mediated isomerization of nitromethane into methyl nitrite prior to dissociation. The studies were extended for the C-2, C-3, and C-4 systems to generalize the idea of isomerization of nitro compound to nitrite prior to dissociation. The studies suggested that the C-2 and the C-3 system predominates via the isomerization channel to give NO as a product despite the fact that the

CME channel threshold is lower. Nitrobutane, however, show some distinct behavior than the C-2 and C-3 systems. The reason may be the presence of a 6-membered transition state or another pathway for the C-4 system which is not available for the C-2 and C-3 systems. Even though roaming reactions are more popular from the ground electronic state dissociations, NO_3 molecule was reported roaming dissociations on an excited electronic. The two experimental sets carried out to understand the photodissociation of NO_3 shows the roaming type dissociation of both D_0 and D_1 surfaces while suggesting a possible different dissociation pathway for the excited NO_3. In the study of IRMPD of vinyl chloride, translational energy distributions suggest that vinyl chloride dissociate via the 3-C transition state while giving vibrationally and rotationally cold vinylidene as a product.

AUTOBIOGRAPHICAL STATEMENT

RAVIN LAKSHITHA FERNANDO

Education

07/2016 Ph.D., Chemistry, Wayne State University.
09/2010 B.Sc., Chemistry, University of Colombo.
09/2008 Grad.Chem;A.I.Chem, Institute of Chemistry Ceylon.

Awards and Honors

2015 Wilfried Heller Research Fellowship.
2014 Graduate School recognition for Exceptional Teaching Service.
2013 Departmental Citation for Excellence in Teaching Service.
2012 Departmental Citation for Excellence in Teaching Service.

Recent Publications

1. Weeraratna, C.; Amarasinghe, C.; Fernando, R.; Tiwari, V.; Suits. A. G.; "Convenient (1+ 1) probe of S (1 D 2) and application to photodissociation of carbonyl sulfide at 216.9 nm." *Chemical Physics Letters* 657 (**2016**): 162-166.

2. Fernando, R.; Ariyasinghe, N.; Suits, A. G.; Imaging NO Elimination in the infrared Multiphoton Dissociation of Nitroalkanes and Alkyl Nitrites. *Chemical Physics Letters.* **2016,** 645: p. 76-83.

3. Fernando, R.; Qu, C.; Bowman, J. M.; Field, R. W.; Suits, A. G., Does Infrared Multiphoton Dissociation of Vinyl Chloride Yield Cold Vinylidene? *The Journal of Physical Chemistry Letters* **2015,** *6* (13), 2457-2462.

4. Fernando, R.; Dey, A.; Broderick, B. M.; Fu, B. N.; Homayoon, Z.; Bowman, J. M.; Suits, A. G., Visible/Infrared Dissociation of NO3: Roaming in the Dark or Roaming on the Ground? *J Phys Chem A* **2015,** *119* (28), 7163-7168.

5. Dey, A.; Fernando, R.; Suits, A. G., State-resolved imaging of CO from propenal photodissociation: Signatures of concerted three-body dissociation. *The Journal of Chemical Physics* **2014,** *140* (15), 154301.

6. Dey, A.; Fernando, R.; Abeysekera, C.; Homayoon, Z.; Bowman, J. M.; Suits, A. G., Photodissociation dynamics of nitromethane and methyl nitrite by infrared multiphoton dissociation imaging with quasiclassical trajectory calculations: Signatures of the roaming pathway. *The Journal of Chemical Physics* **2014,** *140* (5), 054305.

7. Homayoon, Z.; Bowman, J. M.; Dey, A.; Abeysekera, C.; Fernando, R.; Suits, A. G., Experimental and Theoretical Studies of Roaming Dynamics in the Unimolecular Dissociation of CH3NO2 to CH3O + NO. *Z Phys Chem* **2013,** *227* (9-11), 1267-1280.